Fluvial sedimentation and its reservoir potential at foreland basin margins: A case study of the Puig-reig anticline (South-eastern Pyrenees)

Xiaolong Sun[a*], Juan Alcalde[b], Enrique Gomez-Rivas[a], Amanda Owen[c], Albert Griera[d], Juan Diego Martín-Martín[a], David Cruset[b], Anna Travé[a]

[a] *Departament de Mineralogia, Petrologia i Geologia Aplicada, Facultat de Ciències de la Terra, Universitat de Barcelona (UB), c/ Martí i Franquès s/n, Barcelona, 08028, Spain.* xiaolong.sun@ub.edu, e.gomez-rivas@ub.edu, juandiegomartin@ub.edu, atrave@ub.edu

[b] *Geosciences Barcelona (GEO3BCN-CSIC), Lluís Solé i Sabarís s/n, Barcelona, 08028, Spain.* jalcalde@geo3bcn.csic.es, dcruset@geo3bcn.csic.es

[c] *School of Geographical and Earth Sciences, University of Glasgow, University Avenue, Glasgow, 8NN, UK.* amanda.owen@glasgow.ac.uk

[d] *Departament de Geologia, Universitat Autònoma de Barcelona, Bellaterra (Cerdanyola del Vallès), 08193, Spain.* albert.griera@uab.cat

** Corresponding author:* xiaolong.sun@ub.edu

This paper is a non-peer reviewed preprint submitted to EarthArXiv. This preprint has been submitted for publication in a scientific journal on 9th May 2021.

Fluvial sedimentation and its reservoir potential at foreland basin margins: A case study of the Puig-reig anticline (South-eastern Pyrenees)

Xiaolong Sun[a*], Juan Alcalde[b], Enrique Gomez-Rivas[a], Amanda Owen[c], Albert Griera[d], Juan Diego Martín-Martín[a], David Cruset[b], Anna Travé[a]

[a] Departament de Mineralogia, Petrologia i Geologia Aplicada, Facultat de Ciències de la Terra, Universitat de Barcelona (UB), c/ Martí i Franquès s/n, Barcelona, 08028, Spain

[b] Geosciences Barcelona (GEO3BCN-CSIC), Lluís Solé i Sabarís s/n, Barcelona, 08028, Spain

[c] School of Geographical and Earth Sciences, University of Glasgow, University Avenue, Glasgow, 8NN, UK

[d] Departament de Geologia, Universitat Autònoma de Barcelona, Bellaterra (Cerdanyola del Vallès), 08193, Spain

Abstract: Fluvial fans represent one of the dominant sedimentary systems at the active margins of non-marine foreland basins. The Puig-reig anticline at the north-eastern margin of the Ebro Foreland Basin (SE Pyrenees, Spain) exposes continuous outcrops of late Eocene-early Oligocene fluvial deposits, from proximal to medial fluvial fan environments. The proximal deposits, located in the northern limb of the anticline, especially in the northwest zone, are characterised by conglomerates with minor interbedded sandstones, which present thick and wide sheet-like geometries with unscoured or scoured basal surfaces. These are interpreted to be the deposits of unconfined flash floods and wide-shallow channel streams. The medial deposits, covering the rest of the anticline, consist of interbedded beds of conglomerates, sandstones and claystones, deposited from braided channel streams and overbanks. Distal deposits are found towards the south, beyond the anticline, and are characterised by sandstone and clay deposits of terminal lobes or lacustrine deltas and interdistributary bays. This study assesses the impact of the primary depositional characteristics, diagenesis and deformation of the most heterolithic portion of the system, with implications for the understanding of folded fluvial reservoirs. Diagenetic processes, mainly mechanical compaction and calcite cementation, resulted in overall low matrix porosity, with limited relatively higher porosity developed in sandstone lithofacies in the medial deposits. Deformation associated with thrusting and fold growth resulted in the formation of abundant fractures, with relatively higher fracture intensities observed in sandstone lithofacies in the anticline crest. This study shows that post depositional processes can both improve and diminish the reservoir potential of basin proximal fluvial deposits, by the development of open fracture networks and by compaction-cementation, respectively. The comparison of the Puig-reig anticline with other similar settings worldwide shows that foreland basin margin locations can be potential areas for effective reservoirs, even in the case of low matrix porosity.

Keywords: fluvial fans, braided-stream flows, reservoir potential, Ebro Foreland Basin, Pyrenees.

1 Introduction

Reservoirs in foreland basins and adjacent fold-and-thrust belts host some of the most significant hydrocarbon resources in the world , e.g., the Zagros fold-and-thrust belt, the Persian Gulf, the Amu-Darya Basin, the Tarim Basin, the Permian Basin (Mann et al., 2003; Wang et al., 2016), which are also one of the primary targets for low-carbon technologies such as carbon capture and storage (CCS) (Sun et al., 2020). Alluvial and fluvial fans are the main deposits at active margins of non-marine foreland basins (DeCelles and Cavazza, 1999; Horton and Decelles, 2001; Ventra and Clarke, 2018). Alluvial fans are often dominated by conglomeratic facies, and can be concurrent with flow deposits of larger distributive fluvial systems, which transfer large volumes of coarse and fine sediments across basins (Williams et al., 1998; Weissmann et al., 2013, 2015). These coarse clastic belts tend to present relatively restricted radial extent and show high architectural unpredictability due to the lack of viable conceptual models. Thus, hydrocarbon exploration and development at continental basin margins are generally considered to have high risk and low return (Moscariello, 2018). However, alluvial fan and fluvial fan successions at basin margins have good preservation potential if the subsidence rate creates sufficient space to accommodate the significant sediment thickness (Moscariello, 2005). Complex sedimentary and structural characteristics at the basin margins can result in strong reservoir heterogeneity. Reservoir quality in such settings is mainly controlled by their sedimentary characteristics, e.g., petrographic characteristics and stratigraphic sequence, as well as the diagenesis and fracturing processes that they experience (e.g., Morad et al., 2010; Taylor et al., 2010; Zhang et al., 2011; Watkins et al., 2018). Due to the limited well data and seismic resolution of subsurface reservoirs, outcrop analogues play an important role in improving the accuracy of reservoir prediction in the subsurface (*e.g.*, Howell et al., 2014), by providing reliable geological conceptual models and quantitative attribute information (Dichiarante et al., 2020). It is therefore essential to systematically study outcropping reservoir analogues to fully understand and predict the distribution and reservoir potential of alluvial-fluvial deposits in the subsurface.

The northern margin of the Ebro Basin and the adjacent South Pyrenean fold-and-thrust belt present multiple alluvial fans and distributive fluvial systems. For example, the Huesca and Luna systems (Upper Eocene to Oligocene) and series of marginal alluvial fans in the northern margin of the central Ebro Basin have been appraised and well documented (Hirst and Nichols, 1986; Nichols and Hirst, 1998; Arenas et al., 2001; Yuste et al., 2004; Luzón, 2005; Nichols, 2005; Donselaar and Overeem, 2008; Martin et al., 2021). Similar Upper Eocene to Oligocene alluvial and fluvial systems develop in the north-eastern margin of the Ebro Basin, such

as the conglomerate-dominated Berga Group developing near frontal thrust sheets that translates into the fluvial Solsona Formation deposits towards the foreland basin (Sáez, 1987; Ford et al., 1997; Williams et al., 1998; Sáez et al., 2007; de Gibert and Sáez, 2009; Barrier et al., 2010). Based on the study of outcrops near the thrust sheets, Williams et al. (1998) interpreted the Berga Group as a type II alluvial fan setting, using the terminology of Blair and McPherson (1994a, 1994b), due to repeated subaerial sheetflood events and mass movements. More recently, combining new outcrops across the Puig-reig anticline, Barrier et al. (2010) identified two distinct alluvial fans in the Berga Group. The first one is a large braided-stream-flow-dominated alluvial fan, which is related to the majority of the Berga Group deposits. The large alluvial fan was fed by a regional drainage basin including the south Pyrenean cover thrust sheets and the Pyrenean Axial Zone (Vergés, 2007). The second one is a small and local alluvial fan, which developed after the first large fan at the top of the Berga Group and is dominated by stream flows and gravity flows. This small alluvial fan was fed by a local drainage basin, extending only on the outermost cover thrust sheets.

The alluvial-fluvial strata show high potential to become effective reservoirs, e.g., the Puig-reig anticline, which was assessed as a potential site for gas storage (Instituto Geológico y Minero de España, 1995). Besides, the well-exposed outcrops can provide excellent reservoir analogues to determine the reservoir potential of folded alluvial-fluvial successions at basin margins. Previous studies of the alluvial-fluvial deposits in the north-eastern Ebro Basin were focused on the description and interpretation of the sedimentary environments and the interactions between sedimentation and tectonic activities (Williams et al., 1998; Sáez et al., 2007; Barrier et al., 2010; Carrigan et al., 2016), whereas these well-exposed outcrops have not been used as analogues to explore the reservoir potential of similar sedimentary systems in the subsurface. In this study, we focus on the Puig-reig anticline, which continuously exposes high-quality outcrops that present variations of sedimentary facies across the structure. We quantitatively describe and interpret the lithofacies and sedimentary facies of the deposits as well as their distribution over the Puig-reig anticline. In addition, we determine the reservoir quality of different lithofacies and their structural positions along the anticline based on a comprehensive analysis of lithology, cement, porosity, fracture distribution to explore the reservoir potential of the studied anticline and other similar systems at basin margins. This allows an assessment of how primary depositional characteristics as well as subsequent diagenetic and tectonic processes may influence the resource and storage potential of basin proximal deposits.

2 Geological setting

The Pyrenees is a doubly verging orogenic belt that formed during the continental collision between the

Iberian and European plates from Late Cretaceous to Miocene (Muñoz, 1992; Vergés et al., 2002). This orogenic belt is characterised by an antiformal stack of basement-involved thrusts (the Axial Zone) surrounded by two fold-and-thrust belts that were transported to the north and south over the Aquitanian (France) and Ebro (Spain) foreland basins, respectively (Choukroune, 1989; Roure et al., 1989; Muñoz, 1992). The eastern part of the Ebro Basin displays an irregular shape bounded by the Pyrenees to the north and the Catalan Coastal Range to the southeast (Fig. 1A, B) (Vergés, 1993). The Vallfogona thrust represents the major frontal thrust between the SE Pyrenean thrust sheets and the Ebro Basin (Vergés et al., 1998). The Busa syncline and the Puig-reig anticline developed along the footwall of the Vallfogona thrust during Late Eocene and Oligocene (Fig. 1B, C) (Vergés, 1993). The Busa syncline developed over a blind thrust flat (Busa thrust) connected to the Vallfogona floor thrust. A geometric reconstruction allowed an interpretation of the Puig-reig anticline as the consequence of a duplex stack in deep (Vergés, 1993). The Puig-reig is a km-scale south-verging gentle anticline with a flat hinge. The fold-trend is ESE/WNW, slightly oblique to the main Pyrenean structures (Vergés, 1993).

The Ebro Basin sediment fill includes synorogenic Paleocene to Oligocene marine to non-marine deposits lying on top of the Paleozoic basement and Mesozoic sediments (Fig. 1C). The lower part of the Puig-reig anticline is mainly composed of deltaic sandstones and marine marls of the Banyoles and Igualada formations (Middle-to-Upper Eocene), which deposited between the Beuda and Cardona evaporitic formations (Vergés et al., 1992; Serra-Kiel et al., 2003a, 2003b). These deposits were followed by alluvial-fluvial sediments of the Berga Group and the Solsona Formation (Upper Eocene to Oligocene), which were deposited during the endorheic stage of the Ebro basin (Puigdefàbregas et al., 1986, 1992) after a rapid transition from marine to continental environments of deposition (Costa et al., 2010). To the north, at the footwall of the Vallfogona thrust, the Berga Group consists of > 2000 m-thick alluvial and proximal fluvial conglomerates interbedded with minor sandstones and claystones, which displays growth strata (Ford et al., 1997; Suppe et al., 1997). To the south, the Berga deposits became progressively finer-grained and thinner-bedded fluvial conglomerates, sandstones and claystones of the Solsona Formation (Williams et al., 1998; Barrier et al., 2010), which translated downstream to distal terminal deposits of the Súria Formation (Sáez et al., 2007). These fluvial deposits graded into evaporites and calcareous lacustrine strata towards the centre of the Ebro Basin, e.g., the Torà, Barbastro, Castelltallat and Calaf formations (Sáez, 1987; Del Santo et al., 2000; Sáez et al., 2007). These formations collectively represent the basin proximal to basin centre facies within an internally drained continent basin. The formation subdivision of the Berga Group used in this study follows the scheme of Williams et al. (1998). In the study area, we focus on the Camps de Vall-Llonga Formation, a sub-unit of the Berga Group, that covers the northern zone of the Busa syncline and a large area of the Puig-reig anticline, and the Solsona Formation that is

mainly observed in the southern limb of the anticline (Fig. 1D, E).

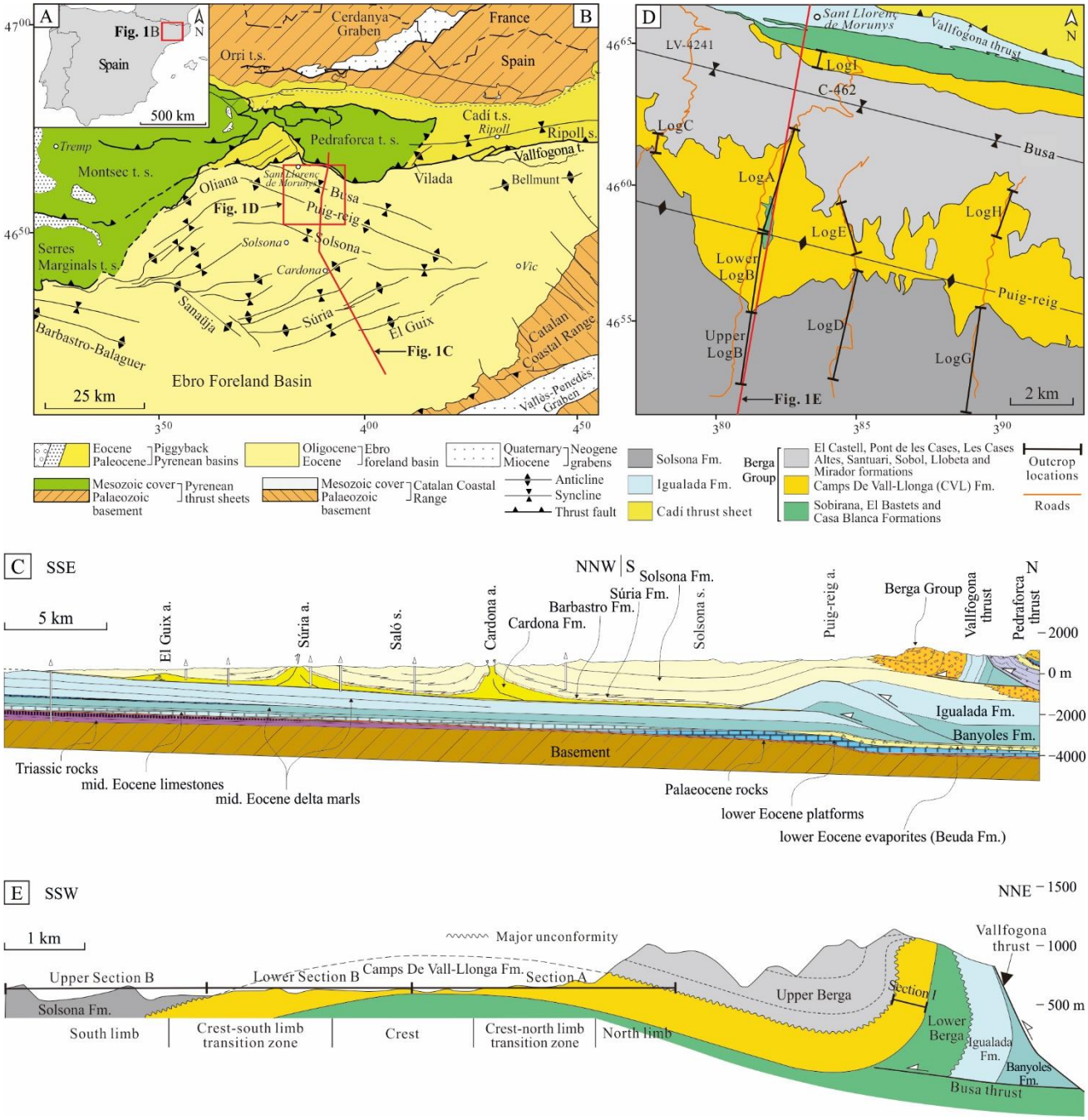

Fig. 1. (A-B) Geographical location and main structural units of the SE Pyrenean fold-and-thrust belt (Vergés, 1993). (C) Geological cross section of the frontal part of the SE Pyrenean fold-and-thrust belt and the Ebro Basin (Vergés, 1993). (D-E) Distribution of the Berga Group and the Solsona Formation and location of outcrops. The strata distribution in Fig. 1D is based on the regional geological map of Catalonia (Institut Cartogràfic i Geològic de Catalunya, 2006). The formation subdivision of the Berga Group follows the scheme of Williams et al. (1998). Fig. 1E is modified from Williams et al. (1998) and Barrier et al. (2010).

3 Outcrops and methods

The Puig-reig anticline presents excellent outcrops along roads that cut through the structure in a roughly north-south direction, between the towns of Sant Llorenç de Morunys in the north and Solsona in the south (Fig. 1B, D). Seven high-resolution (decimetre-scale) stratigraphic logs with a total thickness exceeding 3,000 m were built (Fig. 1D). Among these, logs A, C, E and H and the lower portion of log B represent the strata of the Camps de Vall-Llonga Formation, while logs D and G and the upper portion of log B correspond to the Solsona Formation. The ca. 9 km-long geological cross-section of the Puig-reig anticline (sections A and B, Fig. 1E) is roughly parallel to the N-S shortening direction of the South-eastern Pyrenees and displays the continuous transition from proximal to relatively distal deposits. Moreover, log I of the Camps de Vall-Llonga Formation in the northern zone of the Busa syncline from Barrier et al. (2010) was utilised in this study for comparison. The detailed sedimentary data acquired include bedding thickness, grain size, sedimentary structures and presence of bioturbation, which collectively allow the identification of sedimentary facies and facies associations. The Puig-reig anticline was divided into five structural positions from north to south (i.e., north limb, crest-north limb transition zone, crest, crest-south limb transition zone and south limb; Fig. 1E). The terms 'proximal' and 'distal' were not used to name the structural positions as in other studies (*e.g.*, Ge et al., 1997; Martínez-Martínez et al., 2002) to avoid potential confusions with sedimentary system terms used to divide facies and environments of deposition (i.e., proximal, medial and distal).

To determine rock composition, diagenetic alteration and porosity, 108 polished thin sections from host rocks and calcite veins were made from collected samples. These samples are representative of the different sedimentary lithofacies that can be defined in the area and different structural positions of the anticline. Petrographic observations were taken using a Zeiss Axiophot optical microscope and a Technosyn Cold Cathodoluminescence microscope, model 8200 Mk5-1 operating 16 to 17 kV and 270 to 290 μA gun current. Among these, 30 sandstone thin sections were selected for rock composition analysis using the point-counting method (300-400 points) to reveal potential compositional variations in different sedimentary lithofacies. In total, 60 thin sections were analysed using NIS Elements and Image J software (Schneider et al., 2012) to quantitatively process microphotographs to determine cement contents and matrix porosity. Based on the colour differences between different components, matrix porosity was determined using microphotographs in parallel nicols, while cement contents were determined using microphotographs in cathodoluminescence. To quantitatively analyse the effect of diagenetic alteration on porosity loss, the original porosity (P_o) of different lithologies was calculated based on Scherer's empirical formula (Scherer, 1987), and the proportion of original porosity destroyed by cementation (PL_{cem}) and by compaction (PL_{com}) of different lithologies were calculated

based on Houseknecht's formulas (Houseknecht, 1987):

$$P_o = 20.91 + 22.9/S_o \quad (1)$$

$$PL_{cem} = \frac{P_{cem}}{P_o} \times 100\% \quad (2)$$

$$PL_{com} = (P_o - P_{cem} - \mathrm{P}_r)/P_o \times 100\% \quad (3)$$

where S_o is the Trask sorting coefficient of grain size, whose values of different lithologies were acquired from grain size analysis data from Sun (2018); P_{cem} is cement content; and P_r is residual porosity.

Abundant fractures were observed in the folded sediments of the Puig-reig anticline due to intensive tectonic deformation, which could exert a significant effect on their reservoir potential as important fluid migration pathways and storage space. The data and analysis of the fracture networks in the Puig-reig anticline from (Sun et al., 2021) were incorporated into this study to comprehensively analyse the reservoir potential in the anticline.

4 Results

4.1 Sedimentology

Eight lithofacies were identified based on lithological characteristics and sedimentary structures, including three conglomerate facies, four sandstone facies, and one fine-grained facies (Table 1), which can combine into six lithofacies associations.

Table 1. Subdivision and description of typical lithofacies.

Lithofacies	Description
Gs1	pebble to boulder, occasional outsize clasts, very poor sorting, clast- to reddish matrix-supported, mainly massive structure and minor rough-stratified structure, unscoured or slightly scoured basal surface, sheet-like geometry
Gs2	pebble to cobble, poor sorting, clast-supported, grey to reddish sand matrix, mainly massive structure, slightly or deep scoured basal surface, sheet-like geometry
Gch	pebble to cobble, moderate to poor sorting, clast-supported, massive structure, scoured basal surface, channelised geometry
Smi	fine to coarse sandstone, mainly massive structure, tabular geometry or sandstone lens, limited burrows
Sm	mainly medium and coarse sandstone, massive structure, tabular geometry, limited burrows
Sl	mainly fine to very fine sandstone, mainly parallel bedding structure and minor cross bedding structure, tabular geometry, common burrows
Sch	medium to coarse sandstone, scattered gravelly clasts or muddy rip-up clasts, massive structure, channelised geometry
F	claystone to siltstone, tabular geometry, intensive weathering, erosion and pedogenesis, very common trace fossils

4.1.1 Lithofacies

Conglomerate lithofacies (Gs1, Gs2 and Gch)

The conglomerate lithofacies is subdivided into three subfacies (Gs1, Gs2 and Gch), based on subtle internal lithological differences. All subfacies have polygenic clasts composed of carbonate, siliciclastic, igneous and

metamorphic lithologies. In subfacies Gs1, the clasts consist of very poorly sorted and subrounded pebbles to small boulders, with occasional outsize carbonate clasts. This lithofacies is clast- to matrix-supported. The matrix consists of reddish sands to small pebbles and lacks clays (Fig. 2A). Gs1 conglomerate bodies tend to present a massive structure and minor rough-stratified layers, unscoured or slightly scoured basal surfaces, and a sheet-like geometry. The thickness of a single bed can range from 1 to 6 m, while bed associations can be up to around 50 m. Horizons can be traced over several kilometres using satellite imagery. Gs1 is only found in the upper part of log C, in the northwest zone of the Puig-reig anticline.

Subfacies Gs2 has relatively smaller grain size and lower matrix content compared to subfacies Gs1, and stratified structure and unscoured basal surfaces are rarely observed. This lithofacies is composed of poorly sorted and subrounded pebbles to cobbles. It is mainly clast-supported and contains grey to reddish matrix of fine to coarse sands (Fig. 2B). Gs2 conglomerate bodies are massive, and have a slightly or deep scoured basal surface, and a sheet-like geometry. The thickness of a single bed generally ranges between 1 and 5 m, while bed associations can be up to around 50 m. Gs2 develops in the northern limb, mainly in log C and the upper part of logs A and E.

Subfacies Gch consists of moderately to poorly sorted and subrounded pebble to small cobble size clasts, which tend to be clast-supported with grey, fine to coarse sand matrix (Fig. 2C). Gch conglomerate bodies generally present a channelised geometry and deep scoured basal surfaces, which differ from Gs1 and Gs2 conglomerate bodies. Gch presents lateral wedge-out and changes laterally and vertically to sandstones and claystones. The thickness of a single bed generally ranges from 0.5 to 4 m. Gch is the most widespread conglomerate lithofacies, which develops in most areas of the anticline except for the southern limb.

Sandstone lithofacies (Smi, Sm, Sl and Sch)

Subfacies Smi includes reddish to grey, medium and coarse sandstones and minor fine sandstones. These sandstone layers tend to present a massive structure with locally scattered gravel clasts of a few millimetres in size, and in some minor cases parallel-bedding can be observed. The thickness of Smi ranges from 0.2 to 2 m. They can present a tabular geometry interbedded with Gs2 (Fig. 2D) or occur as sandstone lenses within Gs1 and Gs2 conglomerate bodies that rapidly pinch out laterally (Fig. 2E). Very limited large (with diameter up to 1.5 cm) vertical or oblique burrows are observed in these coarse sand deposits. Smi mainly develops in the northern limb of the anticline.

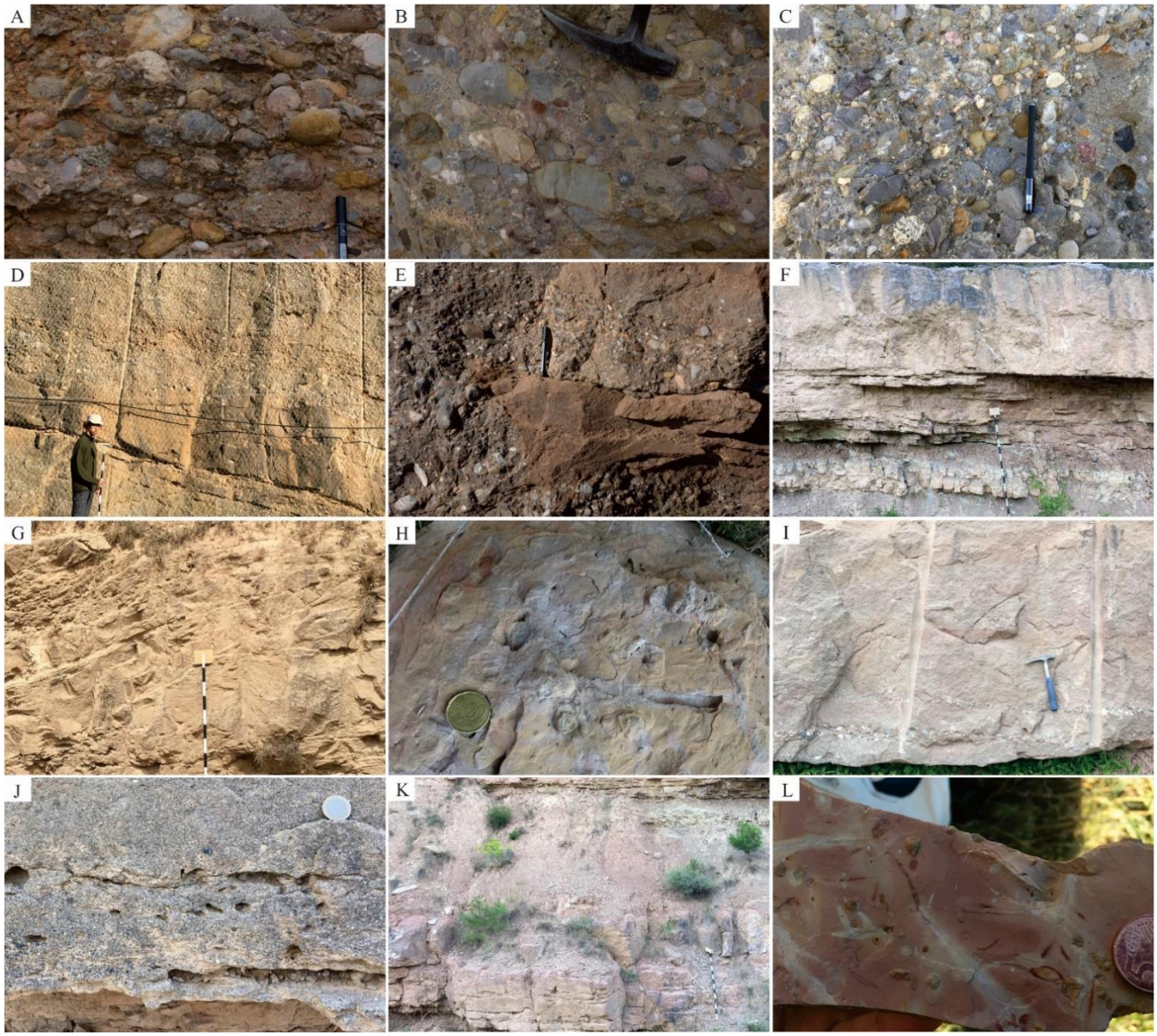

Fig. 2. Field images illustrating typical lithofacies and sedimentary characteristics. (A) Gs1: clast- to reddish matrix-supported pebble to small boulder conglomerate. (B) Gs2: clast-supported pebble to cobble conglomerate with reddish to grey matrix. (C) Gch: clast-supported pebble to small cobble conglomerate with grey sand matrix. (D-E) Smi: reddish to grey massive medium to coarse sandstone extending laterally or pinching out as sandstone lenses. (F) Sm: massive coarse or medium sandstone; Sl: parallel bedding fine sandstone. (G) Sl: cross-bedding fine sandstone. (H) Burrows in fine sandstone. (I) Sch: channelised pebbly coarse sandstone body. (J) Sch: muddy rip-up clasts in the bottom of channelised pebbly coarse sandstone. (K) F: reddish fine deposits with pedogenic characteristics. (L) Abundant trace fossils in fine-grained deposits.

Subfacies Sm is mainly composed of grey, medium and coarse sandstones. Sm sandstone layers tend to present a massive structure with bedding thickness ranging from 0.5 to 1.5 m (Fig. 2F). They show a tabular geometry with sharp and unscoured basal surfaces. They are commonly found above Gch layers or interbedded with laminated fine sandstones. Burrows are uncommon in these coarse sandstone layers, similarly to Smi layers. Sm is one of the dominant lithofacies and is widely observed across the anticline.

Subfacies Sl is composed of grey, fine to very fine sandstones and minor medium sandstones. Parallel-bedding is the most common structure (Fig. 2F), while cross-bedding is occasionally observed (Fig. 2F). Sl tends to be interbedded with Sm and fine deposits. Vertical, oblique or horizontal burrows are more commonly present in these fine sandstones (Fig. 2H). Sl is another dominant lithofacies and widely developed across the anticline.

Sch is composed of grey, medium to coarse sandstones, with scattered gravelly clasts (Fig. 2I, J). It has a similar massive structure as Sm layers, but has a channelised geometry with scoured surfaces and generally develops at the bottom of lithofacies association. Muddy rip-up clasts are sometimes present at the bottom of Sch due to the scour and re-deposition of fine deposits (Fig. 2J). Sch mainly develops in the southern limb of the anticline.

Fine-grained lithofacies (F)

Lithofacies F includes reddish to grey siltstones and claystones. They occur as tabular bodies and are commonly interbedded with Sm and Sl (Fig. 2K). Small burrows and other trace fossils, e.g., *Taenidium barretti* and *Helminthoidichnites* (de Gibert and Sáez, 2009) are very common in these fine deposits (Fig. 2L). These deposits tend to be affected by intensive weathering, erosion and pedogenesis. Lithofacies F is widely developed across the anticline.

4.1.2 Lithofacies associations and sedimentary environments

Unconfined flash flood deposits with no overbanks (LAp1)

LAp1 association is dominated by lithofacies Gs1 with limited Smi interlayers that generally pinch out laterally as sandstone lenses (Figs. 3A, 4), which combine into large and structureless sheet-like bodies of coarse deposits with unscoured or slightly scoured basal surfaces. These characteristics collectively represent unconfined flow of a flashy nature (Blair and McPheerson, 1994; Nichols and Hirst, 1998; Williams et al., 1998). This association is dominantly found in the northwest portion of the Puig-reig anticline, i.e., the upper part of log C.

Unconfined flash flood deposits and wide-shallow channel deposits with limited overbanks (LAp2)

LAp2 association is composed of lithofacies Gs2, Smi and limited F. Lithofacies Smi and F can occur as stable tabular layers or pinch-out lenses (Figs. 3B, 4). This association presents large and structureless sheet-like geometries, slightly or deep scoured surfaces. These features can collectively represent unconfined flow of a flashy nature or wide-shallow channel flow (Arenas et al., 2001; Yuste et al., 2004; Luzón, 2005). This association is dominantly found in the northern limb of the anticline, mainly in log C and the upper part of logs A and E.

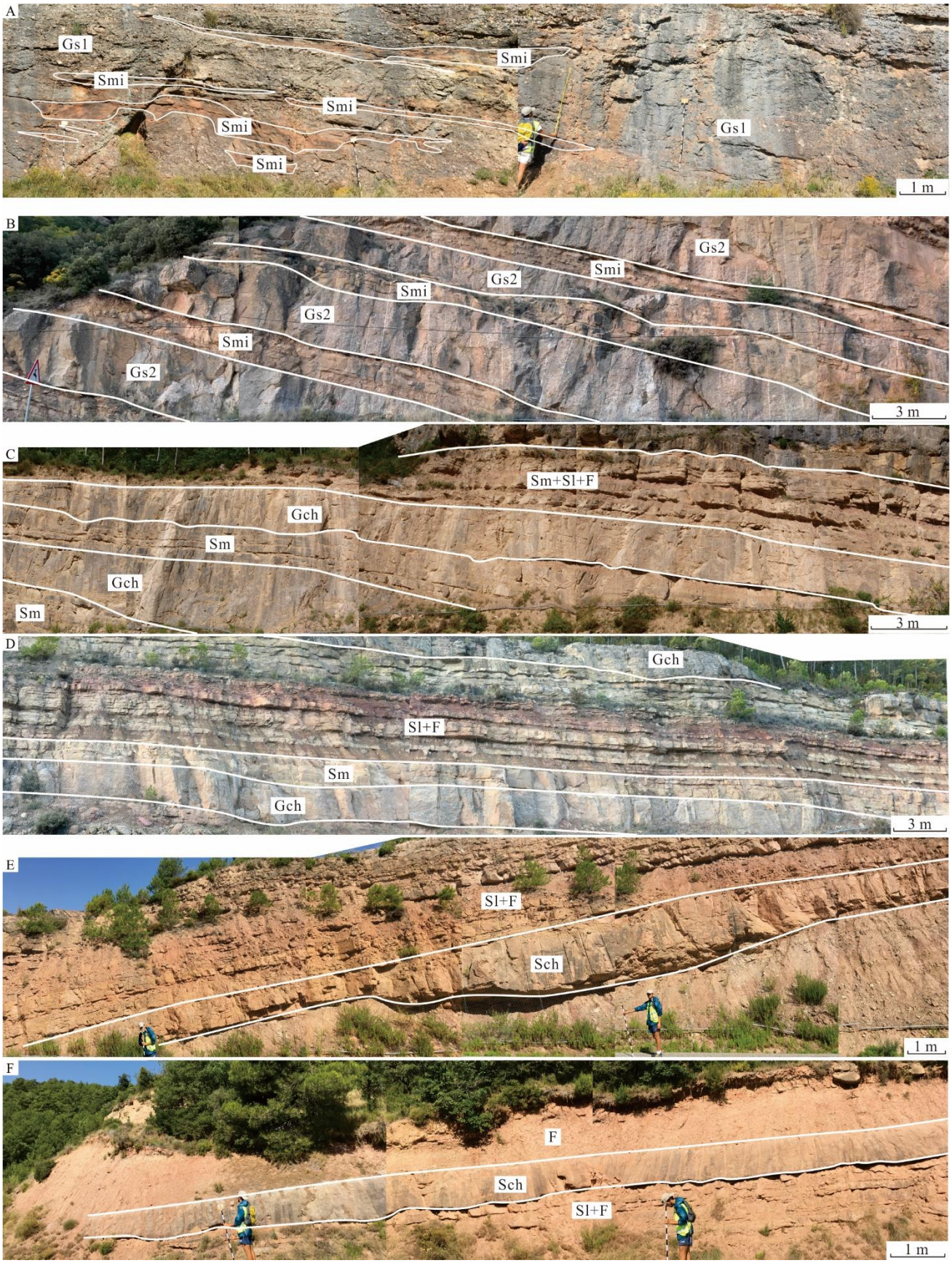

Fig. 3. Field images of typical sedimentary lithofacies associations. (A) LAp1: Gs1 with limited Smi lenses; (B) LAp2: Gs2 with Smi interlayers; (C) LAm1: channel fill Gch, Sm and Sl and minor overbank F; (D) LAm2: Gch channel lag and interlayers of Sm, Sl and overbank F; (E) LAm3: Sch channel lag and interlayers of Sl and overbank F; (F) LAm4: Sl and

stable overbank F incised by Sch channel.

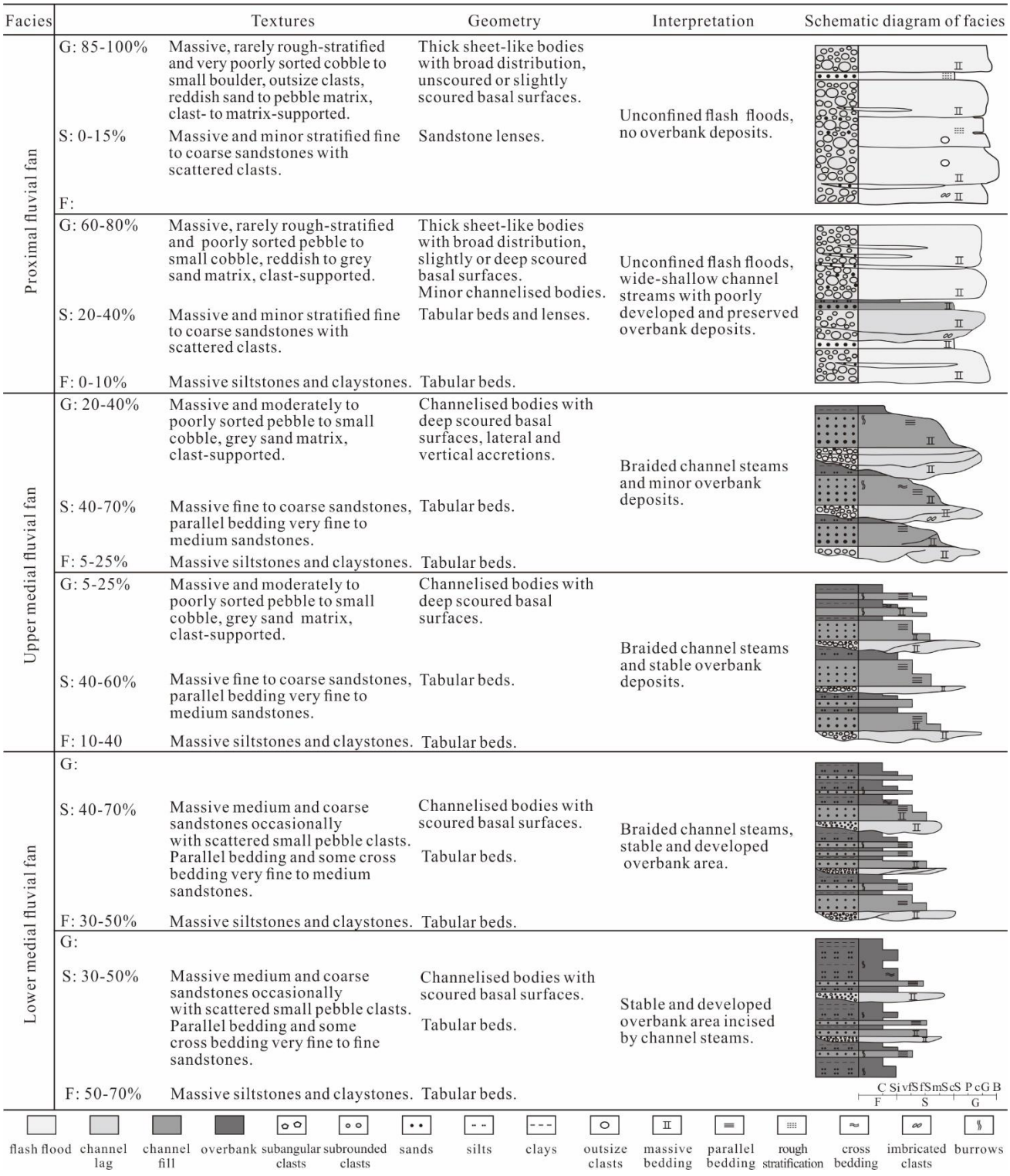

Fig. 4. Summary of sedimentary characteristics of typical lithofacies associations in the Puig-reig anticline. G, S and F refer to the percentage contents of conglomerate, sandstone and fine-grained lithofacies, respectively. C: claystone; Si: siltstone; vfS: very fine sandstone; fS: fine sandstone; mS: medium sandstone; cS: coarse sandstone; P: pebble; cG: cobble; B: boulder.

Channel filling deposits with minor or stable overbanks (LAm1 and LAm2)

LAm1 and LAm2 associations are composed of lithofacies Gch, Sm, Sl, and F. An overall fining-upward trend is observed in these two lithofacies associations, from channelised Gch to tabular and interbedded Sm, Sl and F lithofacies, which collectively represent braided channel streams and overbanks (Nichols and Hirst, 1998; Arenas et al., 2001). LAm1 association is characterised by channel fill deposits with minor overbank deposits, showing vertical or lateral accretions of conglomerates and sandstones (Figs. 3C, 4). LAm2 association is composed of channel fill conglomerates and sandstones and stable overbank fine deposits (Figs. 3D, 4). These lithofacies associations are distributed across the anticline except for the southern limb of the anticline.

Sandy channel filling deposits with stable overbanks (LAm3)

LAm3 association is composed of lithofacies Sch, Sm, Sl and F (Figs. 3E, 4). Compared to LAm1 and LAm2 associations, LAm3 also presents an overall fining-upward trend and is deposited from braided channel streams and overbanks. However, lithofacies Sch with channelised geometries and scoured basal surfaces replaced Gch conglomerate bodies as channel lag deposits. This association is dominantly found in the southern limb and slightly developed in the crest and crest-south limb transition zone of the anticline.

Stable overbanks incised by isolated channels (LAm4)

LAm4 association is composed of lithofacies Sch, Sl and F, which is characterised by stable tabular F and Sl deposits incised by channelised Sch bodies (Figs. 3F, 4). Compared to the LAm3 association, LAm4 also represents channel and overbank deposits, but it contains more overbank fine deposits and isolated channel deposits and does not present a clearly fining-upward trend. This association is occasionally found in the southern limb of the anticline.

The characteristics of the described lithofacies associations (Fig. 4) can collectively represent deposits from a fluvial fan system. The proximal deposits are mainly composed of LAp1 and LAp2 lithofacies associations deposited from unconfined flash floods and wide-shallow channels, with minor LAm1 and LAm2 lithofacies associations. The medial deposits are composed of LAm1 to LAm4 lithofacies associations deposited from braided channel streams and overbanks. The upper medial fluvial fan is mainly composed of LAm1, LAm2 and limited LAm1 associations, while the lower medial fluvial fan is mainly composed of LAm3 and limited LAm2 and LAm4 associations. Based on the distribution of lithofacies (Fig. 5), the conglomerate lithofacies decreases from log C to log H and from log A to log B, log E to log D and log H to log G, respectively. Furthermore, the lithofacies associations present a similar distribution pattern (Fig. 6). LAp1 and LAp2 associations decrease significantly from log C to log H (WNW to ESE) and from log A to log B (north to south), which are replaced by LAm1 and LAm2 and finally translated into LAm3 and LAm4 south-eastward. The distributions of

lithofacies and lithofacies associations are consistent with a fluvial system with an overall south-east downstream trend.

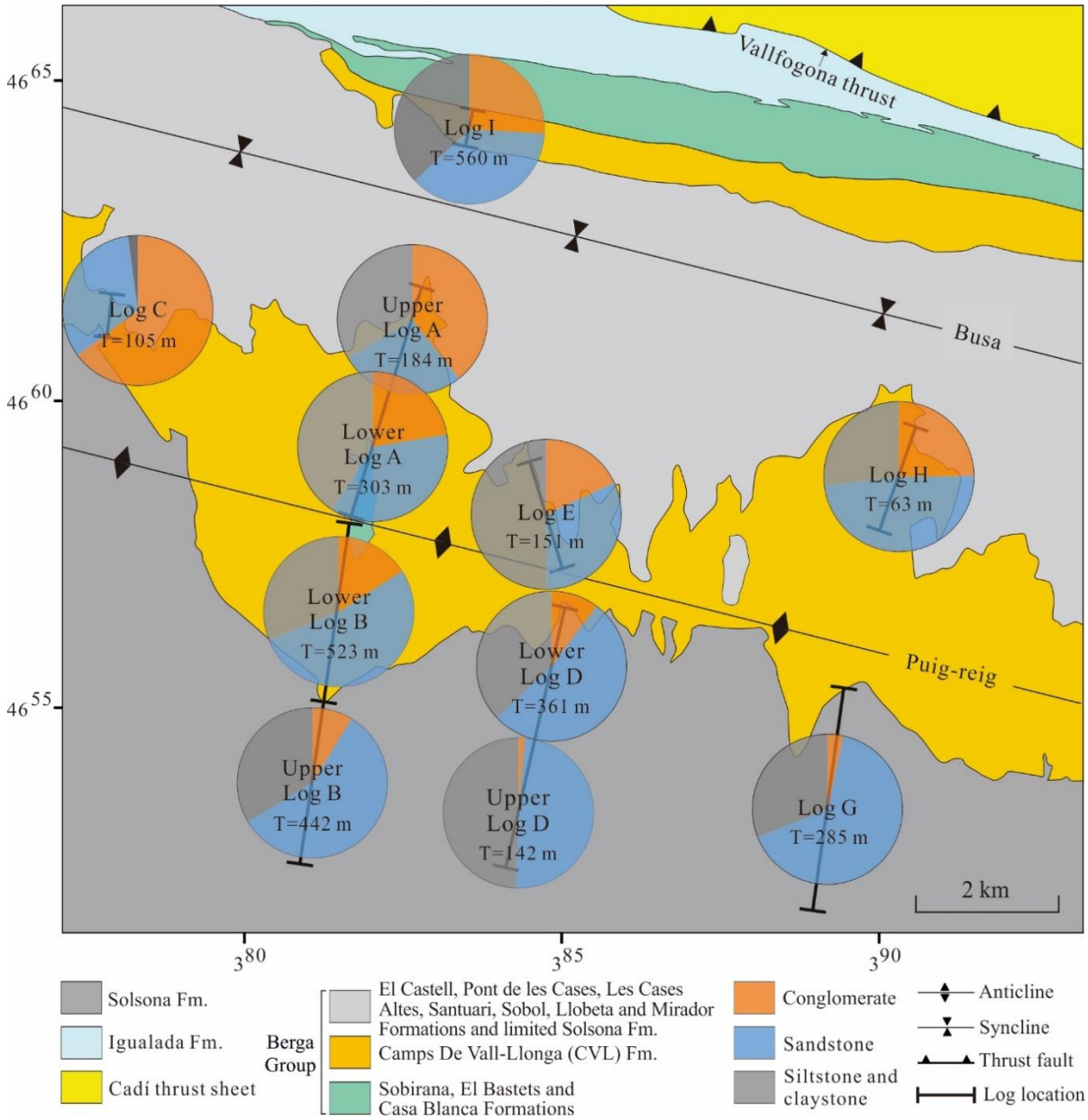

Fig. 5. Percentage distribution of lithofacies (conglomerate, sandstone and fine-grained facies) in the Puig-reig anticline. *T* is the cumulative thickness of deposit layers. Log I is from Barrier et al. (2010).

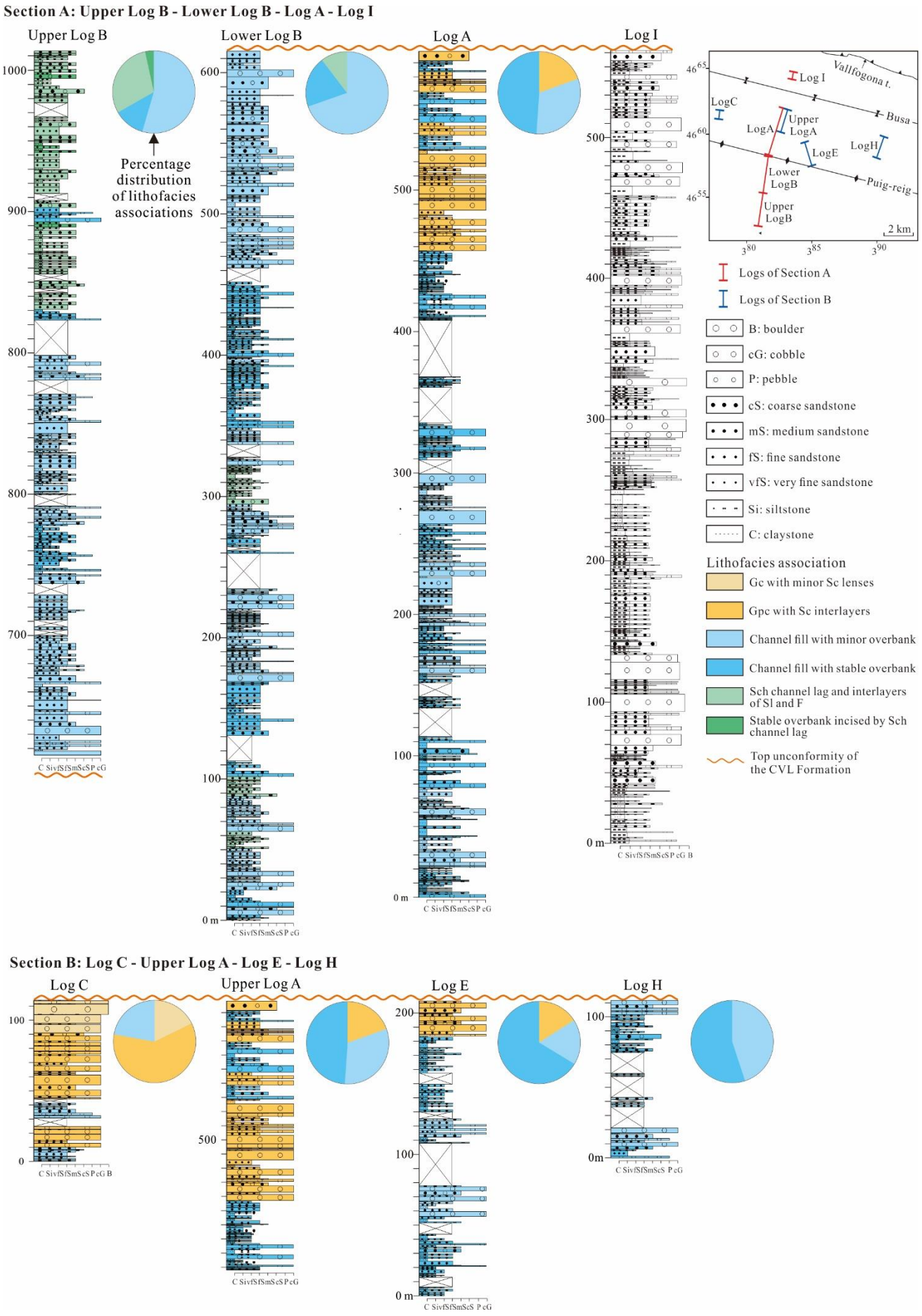

Fig. 6. Correlation of stratigraphic logs and percentage distribution of lithofacies associations in the Puig-reig anticline.

Log I is from Barrier et al. (2010).

4.2 Reservoir characteristics

Based on Folk's (1980) sandstone classification scheme, all sandstone samples of the studied area plot within the litharenite field, with lithic content ranging from 60% to 90%, quartz content ranging from 5% to 30%, and very limited feldspar content (Fig. 7A). Based on Zuffa's (1980) classification scheme of hybrid arenites, these samples mainly plot in the carbonate extrarenite field with minor in the non-carbonate extrarenite field (Fig. 7B). The content of carbonate extrabasinal grains mainly ranges from 40% to 70%, while the content of non-carbonate extrabasinal grains, including non-carbonate lithic, quartz, feldspar, mainly ranges from 30% to 60%. The proximal fluvial fan has a slightly higher content of carbonate extrabasinal grains, compared to the medial fluvial fan. However, as can be seen in Fig. 7, no portion of the fan has a distinctive compositional signature with overlap between the different samples.

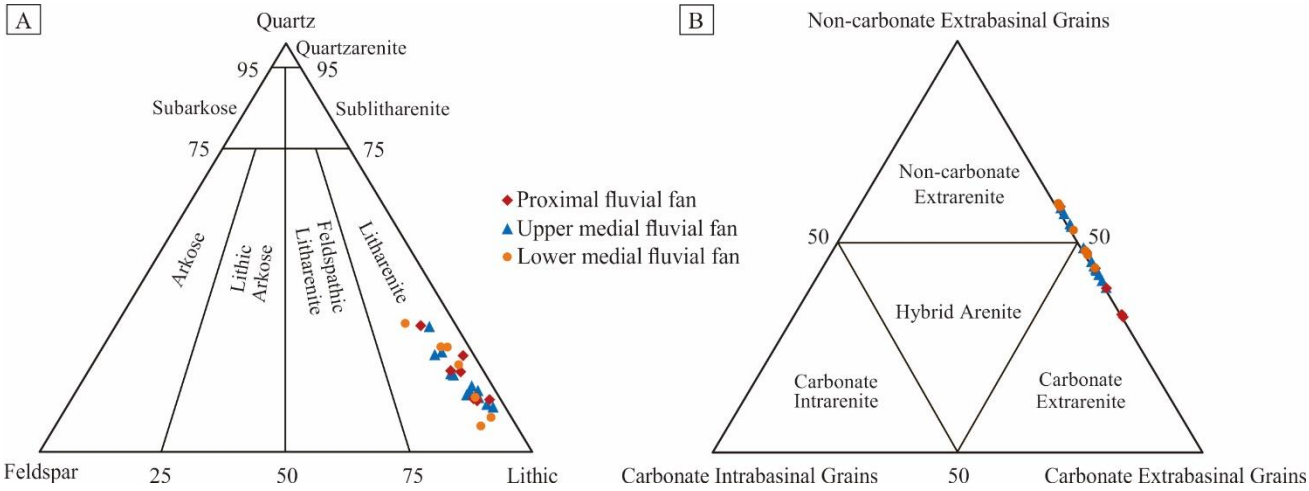

Fig. 7. Classification of sandstones based on framework grain composition after (A) Folk's (1980) and (B) Zuffa's (1980) classification schemes.

Most deposits present very low matrix porosity. Matrix porosity mainly ranges from 0% to 2% (Fig. 8), with an average of 1.2%. It varies across different lithofacies and presents an overall increasing and then decreasing trend with increasing grain size (Fig. 9A). Limited samples present relatively higher matrix porosity concentrated in lithofacies Sch and Sm in the crest, crest-limb transition zones and southern limb of the anticline, mainly ranging from 2% to 8% (Fig. 8). Calcite is the dominant cement mainly ranging from 5% to 15% (Fig. 8), with an average value of 11.6%, which also presents an overall increasing and then decreasing trend with increasing grain size (Fig. 9B). Sandstone lithofacies has slightly higher cement content compared to conglomerate and fine-grained lithofacies, with an average value of 12.7%. There is no clear correlation between cement content and matrix porosity (Fig. 10).

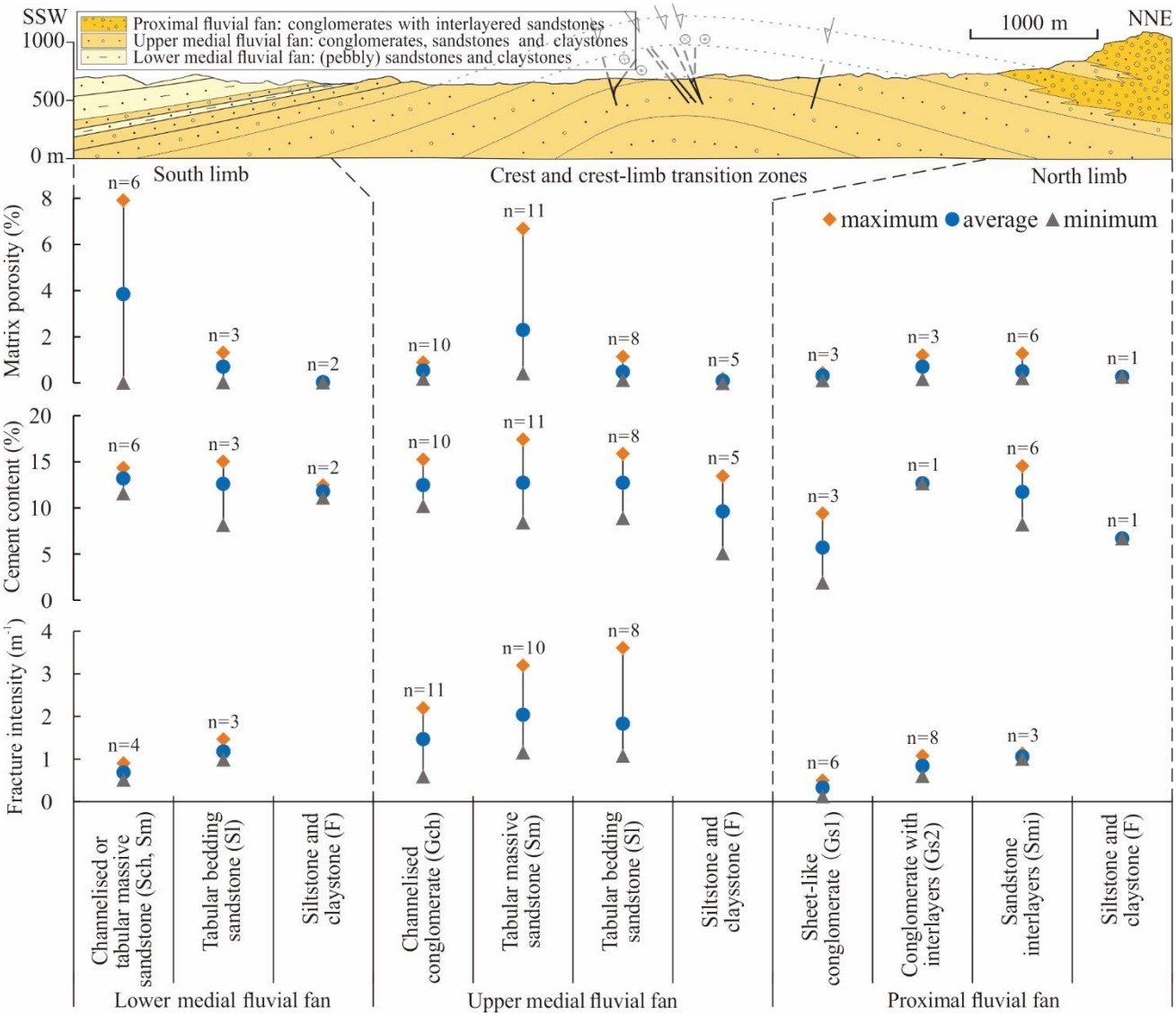

Fig. 8. Distribution of matrix porosity, cement content and fracture intensity in different lithofacies, sedimentary facies and structural positions (*n* is the number of thin sections or fracture scanlines sampling each lithofacies). The cross section is modified from Cruset et al. (2016). Fracture intensity data is from Sun et al. (2021).

Original porosity was calculated based on the Trask sorting coefficient of different lithologies from Sun (2018). Sorting coefficient of siltstone and sandstone mainly ranges from 1.3 to 2.3, resulting in original porosity between 31% to 39% with an average of 35%, while sorting coefficient of conglomerate mainly ranges from 1.6 to 2.6, resulting in original porosity between 30% to 35% with an average of 32%. Cementation and compaction are the most significant diagenetic processes in the Puig-reig anticline. Original porosity destroyed by cementation mainly ranges from 20% to 50%, whereas that destroyed by compaction mainly ranges from 40% to 80% (Fig. 11A, B). Limited samples with relatively high matrix porosity have porosity destroyed by cementation and compaction mainly ranging from 30% to 50% and from 40% to 60%, respectively (Fig. 11A).

Fracture intensity data were obtained from previous research in the Puig-reig anticline (Sun et al., 2021).

Fine-grained lithofacies tend to experience intensive weathering, erosion and pedogenesis and thus impede the identification of fracture attributes in these layers. Thus, fracture attributes were only measured in conglomerate and sandstone lithofacies using the linear scanline method. Fracture intensity mainly ranges from 0.5 m^{-1} to 2.5 m^{-1}, with relatively higher values developed in the crest and crest-limb transition zones of the anticline, especially in sandstone lithofacies with values larger than 1 m^{-1} (Fig. 8). Fracture intensity decreases with increasing distance to anticline hinge and with increasing bedding thickness (Fig. 9C, D).

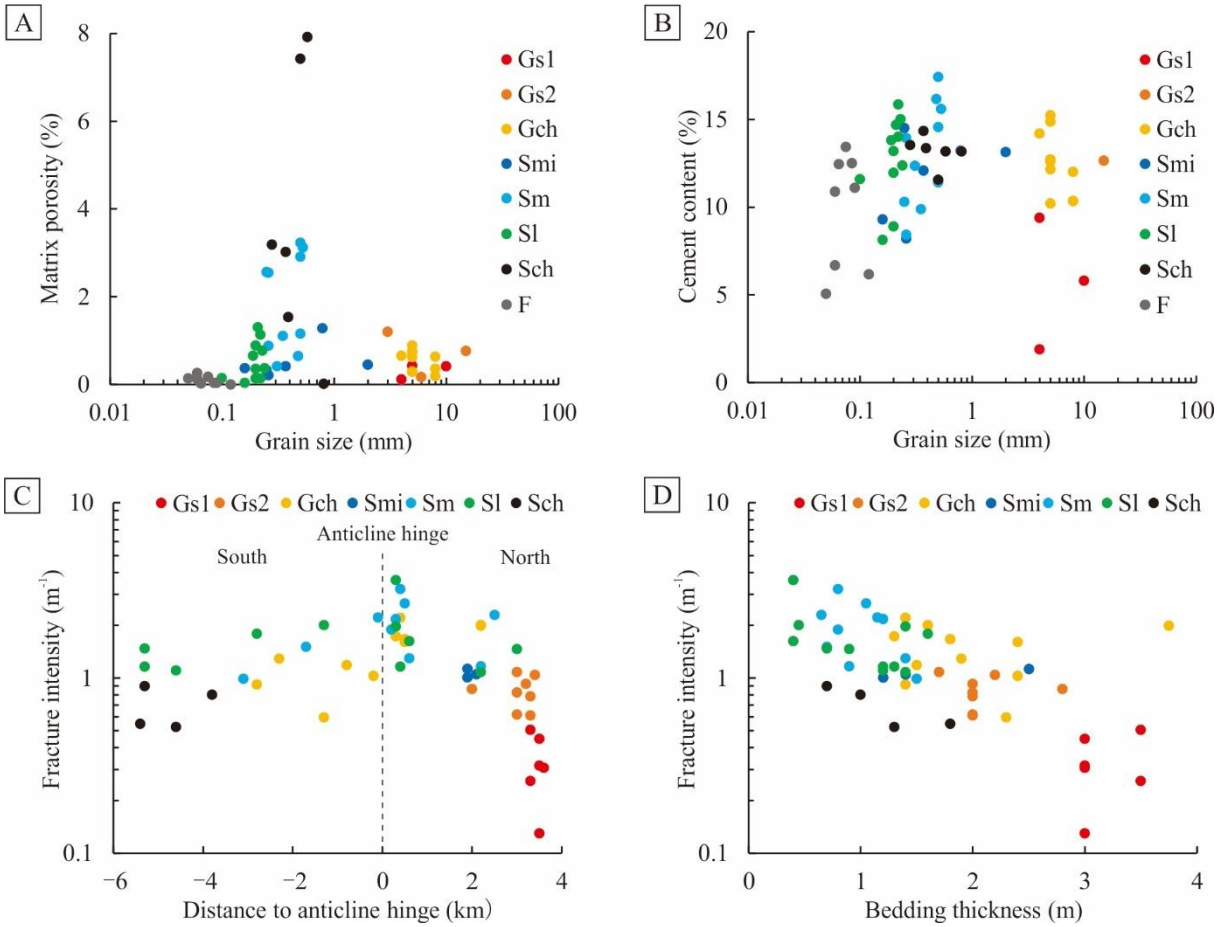

Fig. 9. Crossplots between reservoir characteristics and sedimentary characteristics and structural position. (A) Matrix porosity *vs.* grain size. (B) Cement content *vs.* grain size. (C) Fracture intensity *vs.* distance to anticline hinge. (D) Fracture intensity *vs.* bedding thickness. Fracture intensity data is from Sun et al. (2021).

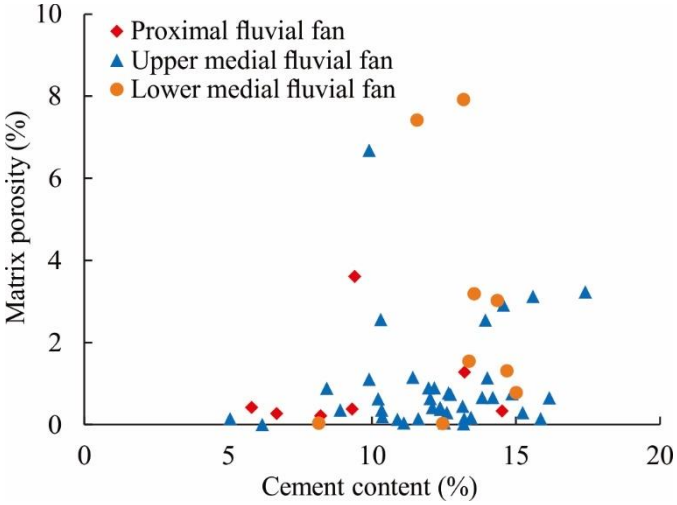

Fig. 10. Crossplot of cement content *vs.* matrix porosity.

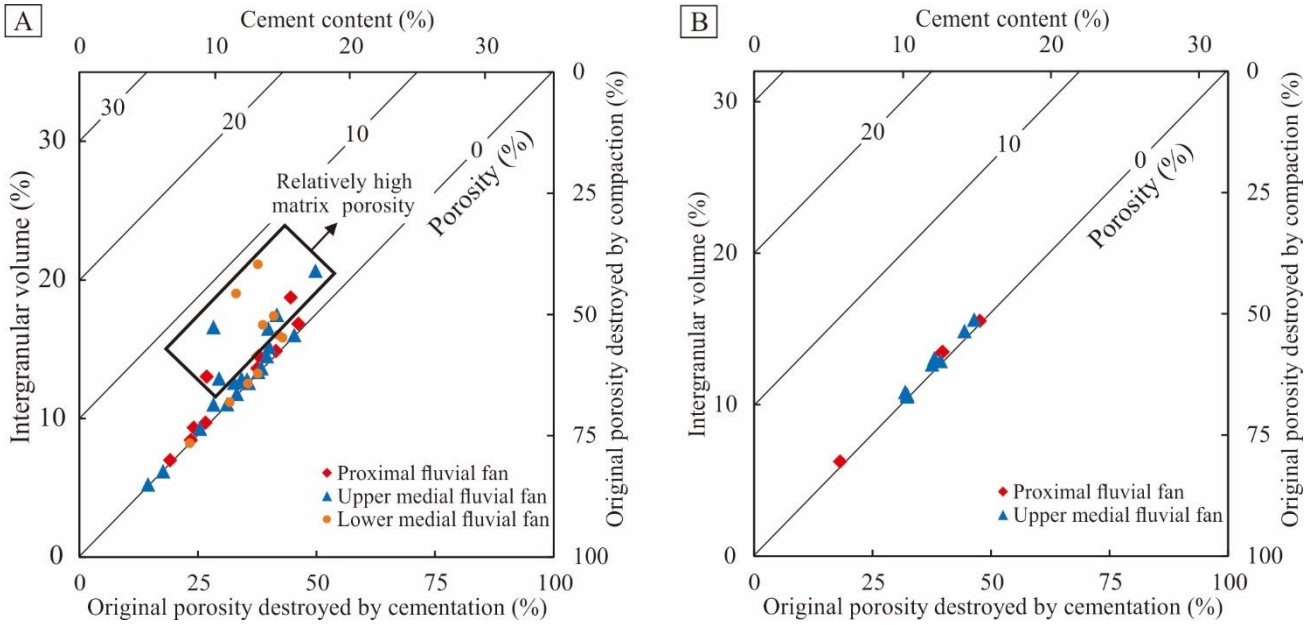

Fig. 11. Crossplots of intergranular volume *vs.* cement content and porosity loss by compaction *vs.* cementation for (A) sandstone and fine-grained lithofacies and (B) conglomerate lithofacies.

5 Discussion

5.1 Fluvial fan sedimentary environments

Previous studies interpreted the whole Berga Group as alluvial fan deposits that wedge out into fluvial fan deposits of the Solsona Formation (Williams et al., 1998; Barrier et al., 2010). However, here we focus on the analysis of the Camps de Vall-Llonga Formation of the Berga Group and the Solsona Formation in the Puig-reig anticline. They are interpreted as deposits of a proximal-medial fluvial fan, based on the comprehensive analyses of the drainage basin, fan size and sedimentary characteristics and the comparison to other similar sedimentary systems in the central Ebro Basin (Hirst and Nichols, 1986; Arenas, 1993; Nichols and Hirst, 1998;

Arenas et al., 2001).

Alluvial fan deposits are sourced by areal-limited drainage basins, whereas fluvial fan deposits tend to have larger drainage basins with long-term expansion and integration of catchments (Moscariello, 2018). The Camps de Vall-Llonga and Solsona deposits are composed of polygenic clasts, including both carbonate and non-carbonate clasts (Fig. 7B). As noted by Riba (1976), the non-carbonate clasts of acid-intermediate plutonic rocks, Permo-Triassic red beds, Carboniferous micro-conglomerates, rare metasedimentary rocks and basic igneous rocks, all come from the basement of the Pyrenean Axial Zone. The varied carbonate clasts reflect source areas in the Mesozoic-Cenozoic series of the south Pyrenean thrust sheets and the Pyrenean Axial zone (Devonian carbonates). The polygenic compositions reveal the drainage basin of the Camps de Vall-Llonga and Solsona deposits extending from the south Pyrenean thrust sheets to the Pyrenean Axial Zone, which is consistent with the large and regional-scale drainage basin of fluvial deposits.

Alluvial fans may range widely in radial length, rarely up to 10 km in exceptional circumstances favouring particularly long runout for sediment-water mixtures (e.g., Blair, 2003), but the radial fans extent generally varies from several hundred metres to a few kilometres at most (Blair and McPheerson, 1994; Moscariello, 2018). The Camps de Vall-Llonga deposits spread over a large area from the Vallfogona thrust to the Puig-reig anticline. The Camps de Vall-Llonga formation is exposed for around 9 km in the direction perpendicular to the Vallfogona thrust and for around 20 km in a direction roughly parallel to the thrust based on the studied outcrops and the regional geological map of the study area (Institut Cartogràfic i Geològic de Catalunya, 2006). Considering the folding of strata and the unexposed strata to the south, the actual extent of the Camps de Vall-Llonga deposits should be larger than the observable extent, which is larger than that of typical alluvial fans. There has been much debate regarding how alluvial fans are distinguished from distributive (fluvial) fan systems (Ventra and Clarke, 2018). In reality, there is likely a continuum between the two systems that the Camps de Vall-Llonga Formation sits close to. However, its size and prevalence of channelised facies indicate that they are the deposits of a distributive fluvial system (fluvial fan).

In the northwest portion of the study area, the Camps de Vall-Llonga Formation is dominated by the proximal deposits from flash floods and wide-shallow channel streams. The development of flash floods in the proximal fluvial fans is also documented in the northern margin fans of the central Ebro Basin (Luzón, 2001, 2005). The channel fill deposits within flash flood conglomerates may have formed during the waning stages of flood events or developed on fan surfaces by later confined flow events (Blair and McPheerson, 1994; Nichols and Hirst, 1998). The rest of the Camps de Vall-Llonga Formation is dominated by the medial deposits from braided channel streams and overbanks. They tend to present an overall fining-upward trend from channel fill

conglomerates and sandstones to overbank fine deposits, representing cyclic (avulsive) behaviour of the system as it developed through time. In the crest-south limb transition zone of the Puig-reig anticline, the Solsona Formation is still dominated by channel fill and overbank deposits. There are no perceptible differences of sedimentary environments in the transition area between the Camps de Vall-Llonga and Solsona formations, i.e., the contact between the upper and lower log B (Fig. 6). In the southern limb, conglomerate channel lags are gradually replaced by (pebbly) sandstone channel lags, i.e., in the upper part of upper log B. We interpret that these deposits still belong to the medial portion of the fluvial fan due to a lack of the terminal deposits of distal fluvial fan and the lacustrine sedimentary characteristics. The Camps de Vall-Llonga and Solsona formations therefore represent mappable units rather than distinct separate sedimentary systems. The distal fluvial deposits can be found 20 km south of our study area. Deposits here are composed of terminal lobes during low lake-level stages and fluvial-dominated deltas and interdistributary bays during high lake level stages, which grades into evaporites and calcareous lacustrine strata near the basin centre (Del Santo et al., 2000; Sáez et al., 2007). Based on observations from the whole Berga Group (Williams et al., 1998), paleocurrents are roughly directed towards the south or southeast, but they also comprise a large component subparallel to the mountain-front structures (Barrier et al., 2010). The decrease of lithofacies associations dominated by conglomerates and the increase of lithofacies associations dominated by sandstones and fine deposits towards the south and southeast (Figs. 5, 6) is consistent with the overall paleocurrents of the Berga Group, supporting the interpretation of fluvial fan deposits.

However, we do not discard the possibility of several alluvial fans developing during the deposition of the Berga Group, which are restricted at the northern basin margin with small fan size and local drainage basins, e.g., the small stream-flow and gravity-flow-dominated alluvial fan identified by Barrier et al. (2010) at the top of Berga Group and located to the northwest in Fig. 1D. This has been observed to be the case in the northern margin of the central Ebro Basin where two distributive systems (the Luna and Huesca fluvial systems) coincide and interfinger with a series of marginal alluvial fans (Hirst and Nichols, 1986; Nichols and Hirst, 1998; Arenas et al., 2001).

5.2 Reservoir potential of the folded fluvial succession in the Puig-reig anticline

Based on the distribution of calcite cement, porosity, fracture intensity and lithology in the Puig-reig anticline, here we discuss the controlling factors of reservoir quality and the reservoir potential of the folded fluvial succession in the Puig-reig anticline in the SE Pyrenees.

Reservoir matrix porosity is mainly controlled by the sedimentary characteristics of deposits and the diagenetic processes they experience (Dos Anjos et al., 2000; Bjørlykke, 2014). In the Puig-reig anticline, the

fluvial deposits present an overall low matrix porosity due to intensive compaction and cementation (Fig. 10), but which varies across the different lithofacies. Relatively high matrix porosity concentrates in lithofacies Sch and Sm in the medial fluvial fan, regardless their relatively higher cement contents with respect to other lithofacies (Fig. 9A, B). Compared to lithofacies Sl and F, Sch and Sm have low contents of ductile matrix. Compared to conglomeratic facies, these medium to coarse sandstones present better grain sorting and lower matrix contents, thus resulting in relatively higher original and residual porosity. Based on the original porosity of sandstone and siltstone (35% on average), the porosity destroyed by compaction of lithofacies Sch and Sm mainly ranges from 40% to 70% with 57% on average, whereas that of lithofacies Sl and F mainly ranges from 55% to 75% with 63% on average and from 60% to 85% with 73% on average, respectively. Lithofacies Sch and Sm experience relatively weaker compaction, resulting in more residual intergranular volume which can provide more space for cementation and residual porosity. This is the main reason for the coexistence of relatively higher residual porosity and calcite content in lithofacies Sch and Sm.

Fracture networks have a significant impact on reservoir performance. According to the systematic analysis of fracture networks in the Puig-reig anticline (Sun et al., 2021), fracture intensity is mainly affected by structural position, bedding thickness (Fig. 9C, D) and lithological association. The crest and crest-limb transition zones present relatively higher fracture intensity due to the greater curvature and finite strain they experience compared to the limbs (Figs. 8, 9C), if a Tangential Longitudinal Strain model (TLS) is assumed (Hudleston and Treagus, 2010). This observation is consistent with some previous studies of fracture distribution in folds (e.g., Iñigo et al., 2012; Awdal et al., 2013; Watkins et al., 2015). If flexural slip was the dominant folding mechanism, then thin and soft layers in limbs would be ones subjected to the highest strain. However, our field data better matches the first option because the anticline crest features more intensive fracturing than the limbs. Relatively thinner sandstone layers tend to present higher fracture intensity than thick conglomerate layers in all structural positions (Figs. 8, 9D), which is also consistent with some previous fracture studies (e.g., Florez-Niño et al., 2005; Wennberg et al., 2007). In addition, the lithological association of competent conglomerate or sandstone and incompetent fine deposits in medial fluvial deposits favour the development of abundant fractures, compared to the lithological association of competent conglomerate and sandstone in proximal fluvial. Based on the analysis above, lithofacies Sl and Sm in the medial fluvial fan located in the crest and crest-limb transition zones of the anticline feature relatively higher fracture intensity than other structural positions and lithofacies.

Based on the distribution of calcite cement, porosity and fracture intensity, the medial fluvial sandstones in the crest and crest-limb transition zones (35-55% of all lithofacies in these zones) present relatively greater

potential to be effective reservoirs due to the high fracture intensity (1-3.5 m^{-1}). The northern limb presents relatively high percentages of sandstone and conglomerate deposits (65-100%) and lower percentages of fine deposits (0-35%), especially in the northwest zone (Fig. 5). However, the sandstone and conglomerate bodies have low potential to become effective reservoirs due to their low matrix porosity (<1.5%) and fracture intensity (<1.2 m^{-1}). The southern limb presents relatively higher percentages of sandstones (50-65%) and very low percentages of conglomerates (0-15%) (Fig. 5). The sandstones have relatively low fracture intensity (<1.5 m^{-1}), but present some reservoir potential in Sch and Sm lithofacies due to relatively higher matrix porosity (3.9% on average).

5.3 Reservoir potential of folded alluvial-fluvial successions at foreland basin margins

As one of the dominant sedimentary systems at the active margins of non-marine foreland basins, alluvial and proximal fluvial fans tend to present heterogeneous reservoir potential due to the interplay between complex sedimentary, diagenetic and deformation processes. Unravelling their reservoir characteristics is therefore key to the success of subsurface operations.

Compared to fluvial fans, alluvial fans present radial-limited fan extent (Blair and McPheerson, 1994). Debris-flow alluvial fans tend to present poor primary reservoir quality due to texturally immature debris deposited from debris flows and hyperconcentrated flows. These deposits have varied reservoir connectivity depending on their abundance in local sedimentary systems (Moscariello, 2018). On the other hand, water-lain alluvial fans, generally dominated by sheet floods, have better reservoir potential due to the presence of relatively better sorted deposits and reservoir connectivity (Moscariello, 2005). At basin margins, proximal fluvial deposits tend to consist of amalgamated channel belts with limited preservation of fine deposits (Weissmann et al., 2013). Thick conglomerate bodies can occur in proximal fluvial deposits (Vincent, 2002), which can be associated with channelised non-cohesive gravity or hyperconcentrated flows (Moscariello, 2018). Besides, flash floods can develop in these proximal fluvial environments, e.g., in the Puig-reig anticline (Fig. 6) and other cases (Luzón, 2001, 2005), resulting in large and coarse sheet-like deposits. Compared to debris-flow alluvial fans, these proximal fluvial deposits can present higher reservoir potential due to their higher textural maturity and better reservoir connectivity. In addition, fluvial deposits at basin margins mainly result from medial fluvial fans, dominated by channel belts with varied overbank fine deposits. Although medial fluvial deposits present a downstream reduction of the reservoir volume and a corresponding increase of overbank fine deposits, they are still dominated by conglomerate or sandstone reservoirs at basin margins and present higher textural maturity resulting in better primary reservoir quality. These water-lain alluvial fans and proximal-medial fluvial fans present high potential to be effective reservoirs without undergoing strong compaction and

cementation.

Intensive diagenesis can result in low matrix porosity and permeability, and thus reduce the reservoir potential in alluvial-fluvial deposits (Morad et al., 2010; Lai et al., 2018). Carbonate cement is one of the prevailing authigenic minerals in these deposits (Hall et al., 2004; Taylor and Machent, 2011). In tectonically active settings, such as foreland basin margins, carbonate extrabasinal grains can become important sediments in alluvial-fluvial systems (Valloni and Zuffa, 1984; Morad et al., 2010). This is because such settings provide short time and distance for sediment transportation and exposure, thus resulting in relatively weak chemical weathering of these carbonate compositions (Zuffa, 1985). These extrabasinal carbonate grains favour the nucleation and growth of carbonate cement in these alluvial-fluvial deposits. In addition, at foreland basin margins, intensive fracturing, thrusting and folding are accompanied with fluid flow of various geological fluids including hydrothermal, meteoric and formation fluids, from which carbonate cement precipitates (Travé et al., 1997, 2000, 2007; Cruset et al., 2018, 2020). Thus, intensive carbonate cementation can result in an overall or localised low matrix porosity of alluvial-fluvial deposits at basin margins, e.g., the Peraltilla and Sariñena formations in the central Ebro Basin (Yuste et al., 2004), the Berga Group and the Solsona Formation in the eastern Ebro Basin (Cruset et al., 2016), the Siwalik Group in the Himalayan Basin (Guilbaud et al., 2012), and the Wuqia Group and the Artux Formation in the south-western Tarim Basin (Zheng et al., 2006). On the other hand, the prevailing carbonate cement can preserve intergranular space and improve reservoir quality by providing secondary porosity under the specific circumstance of intensive dissolution (Al-Ramadan et al., 2004; Hakimi et al., 2012).

At foreland basin margins, fracture networks are widely developed accompanied with intensive deformation in fold-and-thrust belts (Iñigo et al., 2012; Liu et al., 2017). These fracture networks can play a fundamental role both in fluid migration and the resulting reservoir quality, especially in reservoirs with low matrix porosity and permeability (Casini et al., 2011; Watkins et al., 2018; Wang et al., 2020). Fracture intensity can be controlled by multiple factors in folded sedimentary successions, mainly including the sedimentary characteristics and the structural position. Fracture intensity and connectivity tend to be higher in high strain fold crests or forelimbs, such as in the cases of the Puig-reig anticline in the South-eastern Pyrenees (Sun et al., 2021), the Achnashellach Culmination in the Southern Moine Thrust Belt (Watkins et al., 2015), or the Sub-Andean fold-thrust belt (Iñigo et al., 2012). In alluvial-fluvial deposits, variable sedimentary characteristics can exert significant effects on fracture intensity. Proximal fluvial deposits, dominated by large and thick conglomerate and sandstone layers, tend to have lower fracture intensity than medial fluvial deposits, which are defined by interlayered conglomerate or sandstone layers and fine deposits (Sun et al., 2021). This is because fracture intensity tends to present a negative correlation with bedding thickness (Huang and Angelier, 1989;

Florez-Niño et al., 2005). Besides, the interlayered competent conglomerate and sandstone layers and incompetent fine deposits in medial fluvial deposits result in high competence contrast between these distinct mechanical stratigraphic layers, which favours the development of joints or faults (Sibson, 1996; Wilkins et al., 2014). For tight conglomerate and sandstone reservoirs at basin margins, fracture networks can significantly improve reservoir potential (Watkins et al., 2018; Sun et al., 2021).

In summary, compared to deposits in basin centre localities where reservoir quality is mainly controlled by depositional and diagenetic characteristics, basin proximal reservoirs are most likely to be tectonically deformed and feature variable fracture networks. Matrix porosity is mainly controlled by depositional facies and diagenetic, while fracture networks are mainly controlled by depositional characteristics and structural position, e.g., in the Puig-reig anticline (Figs. 8, 9). In the right circumstances an effective combination of both structure and facies can make basin margin locations potential areas for effective reservoirs, even in the case of low matrix porosity.

6 Conclusions

The lithofacies and sedimentary facies of the folded fluvial succession in the Puig-reig anticline, located at the north-eastern margin of the Ebro Foreland Basin (SE Pyrenees), have been analysed to explore the reservoir potential in the studied anticline and other similar systems at basin margins. Based on a comprehensive analysis of lithofacies, porosity, cement and fracture intensity distribution, the following conclusions can be highlighted:

(1) The Camps de Vall-Llonga and Solsona formations in the Puig-reig anticline were deposited as part of proximal-medial deposits of a fluvial fan system. The proximal deposits in the study area are characterised by unconfined flash floods and wide-shallow channel streams. They are dominated by thick and large sheet-like conglomerate bodies with minor interlayered sandstones, and mainly spread in the northern limb of the anticline. The medial deposits are characterised by braided channel streams and overbanks, dominated by the interbedded conglomerates, sandstones and claystones, which finally change to terminal deposits in the distal portion close to the basin centre.

(2) The fluvial deposits present overall low matrix porosity due to intensive compaction and calcite cementation, with relatively high porosity developed in Sm and Sch lithofacies in the medial fluvial fan. Fracture intensity is mainly affected by structural position, bedding thickness and lithological association, with relatively higher values developed in sandstone lithofacies in the high strain zones of the anticline. Sandstone lithofacies deposited in the medial fluvial fan and located in the crest and crest-limb transition zones presents relatively higher potential to be effective reservoirs.

(3) The comprehensive analysis of the Puig-reig anticline can provide an effective analogue for the exploration of subsurface reservoirs. The comparison with other similar settings worldwide shows reservoir potential is comprehensively controlled by sedimentology, diagenesis and deformation at basin margins. An effective combination of both structure and facies can make basin margin locations potential areas for effective reservoirs, even in the case of low matrix porosity.

Acknowledgements

Funding was provided by the Catalan Council to the Grup Consolidat de Recerca "Geologia Sedimentària" (2017SGR-824) and the DGICYT Spanish Project PGC2018-093903-B-C22. XS acknowledges funding by the China Scholarship Council for a PhD scholarship (201806450043). JA is funded by MICINN (Juan de la Cierva fellowship - IJC2018-036074-I). EGR acknowledges funding provided by the Spanish Ministry of Science, Innovation and Universities ("Ramón y Cajal" fellowship RYC2018-026335-I). We thank Enric Sangrà and Francesc Baiget for their support during field campaigns.

References

Al-Ramadan, K.A., Hussain, M., Imam, B., Saner, S., 2004. Lithologic characteristics and diagenesis of the Devonian Jauf sandstone at Ghawar Field, Eastern Saudi Arabia. Mar. Pet. Geol. 21, 1221–1234.

Arenas, C., 1993. Sedimentología y paleogeografía del Terciario del margen pirenaico y sector central de la cuenca del Ebro (zona aragonesa occidental) (Ph.D. thesis). University of Zaragoza, Zaragoza.(in Spanish).

Arenas, C., Millán, H., Pardo, G., Pocoví, A., 2001. Ebro Basin continetal sedimentation associated with late compressional Pyrenean tectonics (North-Eastern lberia): Controls on basin margin fans and fluvial systems. Basin Res. 13, 65–89.

Awdal, A.H., Braathen, A., Wennberg, O.P., Sherwani, G.H., 2013. The characteristics of fracture networks in the Shiranish Formation of the Bina Bawi Anticline; comparison with the Taq Taq Field, Zagros, Kurdistan, NE Iraq. Pet. Geosci. 19, 139–155.

Barrier, L., Proust, J.N., Nalpas, T., Robin, C., Guillocheau, F., 2010. Control of alluvial sedimentation at foreland-basin active margins: A case study from the northeastern Ebro Basin (southeastern Pyrenees, Spain). J. Sediment. Res. 80, 728–749.

Bjørlykke, K., 2014. Relationships between depositional environments, burial history and rock properties. Some principal aspects of diagenetic process in sedimentary basins. Sediment. Geol. 301, 1–14.

Blair, T.C., 2003. Features and origin of the giant Cucomungo Canyon alluvial fan, Eureka Valley, California,

in: Chan, M.A., Archer, A.. (Eds.), Extreme Depositional Environments: Mega End Members in Geologic Time. Geological Society of America Special Papers, 370, pp. 105–126.

Blair, T.C., McPheerson, J.G., 1994. Alluvial fans and their natural distinction from rivers based on morphology, hydraulic processes, sedimentary processes, and facies assemblages. J. Sediment. Res. 64, 450–489.

Blair, T.C., McPherson, J.G., 1994. Alluvial fan processes and forms, in: Abrahams, A.D., Parsons, A.J. (Eds.), Geomorphology of Desert Environments. Springer, Dordrecht, pp. 354–402.

Carrigan, J.H., Anastasio, D.J., Kodama, K.P., Parés, J.M., 2016. Fault-related fold kinematics recorded by terrestrial growth strata, Sant Llorenç de Morunys, Pyrenees Mountains, NE Spain. J. Struct. Geol. 91, 161–176.

Casini, G., Gillespie, P.A., Vergés, J., Romaire, I., Fernández, N., Casciello, E., Saura, E., Mehl, C., Homke, S., Embry, J.C., Aghajari, L., Hunt, D.W., 2011. Sub-seismic fractures in foreland fold and thrust belts: Insight from the Lurestan Province, Zagros Mountains, Iran. Pet. Geosci. 17, 363–282.

Choukroune, P., 1989. The Ecors Pyrenean deep seismic profile reflection data and the overall structure of an orogenic belt. Tectonics 8, 23–39.

Costa, E., Garcés, M., López-Blanco, M., Beamud, E., Gómez-Paccard, M., Larrasoaña, J.C., 2010. Closing and continentalization of the South Pyrenean foreland basin (NE Spain): Magnetochronological constraints. Basin Res. 22, 904–917.

Cruset, D., Cantarero, I., Benedicto, A., John, C.M., Vergés, J., Albert, R., Gerdes, A., Travé, A., 2020. From hydroplastic to brittle deformation: Controls on fluid flow in fold and thrust belts. Insights from the Lower Pedraforca thrust sheet (SE Pyrenees). Mar. Pet. Geol. 120, 104517. https://doi.org/10.1016/j.marpetgeo.2020.104517

Cruset, D., Cantarero, I., Travé, A., Vergés, J., John, C.M., 2016. Crestal graben fluid evolution during growth of the Puig-reig anticline (South Pyrenean fold and thrust belt). J. Geodyn. 101, 30–50.

Cruset, D., Cantarero, I., Vergés, J., John, C.M., Muñoz-López, D., Travé, A., 2018. Changes in fluid regime in syn-orogenic sediments during the growth of the south Pyrenean fold and thrust belt. Glob. Planet. Change 171, 207–224.

de Gibert, J.M., Sáez, A., 2009. Paleohydrological significance of trace fossil distribution in Oligocene fluvial-fan-to-lacustrine systems of the Ebro Basin, Spain. Palaeogeogr. Palaeoclimatol. Palaeoecol. 272, 162–175.

DeCelles, P.G., Cavazza, W., 1999. A comparison of fluvial megafans in the Cordilleran (Upper Cretaceous)

and modern Himalayan foreland basin systems. Bull. Geol. Soc. Am. 111, 1315–1334.

Del Santo, G., Garcia-Sansegundo, J., Sarasa, L., Torrebadella, J., 2000. Estratigrafía y estructura del Terciario en el sector oriental de la cuenca del Ebro entre Solsona y Manresa (NE de España). Rev. la Soc. Geológica España 13, 265–278.(in Spanish with English abstract).

Dichiarante, A.M., McCaffrey, K.J.W., Holdsworth, R.E., Bjørnarå, T.I., Dempsey, E.D., 2020. Fracture attribute scaling and connectivity in the Devonian Orcadian Basin with implications for geologically equivalent sub-surface fractured reservoirs. Solid Earth 11, 2221–2244.

Donselaar, M.E., Overeem, I., 2008. Connectivity of fluvial point-bar deposits: An example from the Miocene Huesca fluvial fan, Ebro Basin, Spain. Am. Assoc. Pet. Geol. Bull. 92, 1109–1129.

Dos Anjos, S.M.C., De Ros, L.F., De Souza, R.S., De Assis Silva, C.M., Sombra, C.L., 2000. Depositional and diagenetic controls on the reservoir quality of Lower Cretaceous Pendencia sandstones, Potiguar rift basin, Brazil. Am. Assoc. Pet. Geol. Bull. 84, 1719–1742.

Florez-Niño, J.M., Aydin, A., Mavko, G., Antonellini, M., Ayaviri, A., 2005. Fault and fracture systems in a fold and thrust belt: An example from Bolivia. Am. Assoc. Pet. Geol. Bull. 89, 471–493.

Folk, R.L., 1980. Petrology of Sedimentary Rocks. Hemphill Publishing Company, Austin .

Ford, M., Williams, E.A., Artoni, A., Vergés, J., Hardy, S., 1997. Progressive evolution of a fault-related fold pair from growth strata geometries, Sant Llorenç de Morunys, SE Pyrenees. J. Struct. Geol. 19, 413–441.

Ge, H., Jackson, M.P.A., Vendeville, B.C., 1997. Kinematics and dynamics of salt tectonics driven by progradation. Am. Assoc. Pet. Geol. Bull. 81, 398–423.

Guilbaud, R., Bernet, M., Huyghe, P., Erens, V., Chirouze, F., Dupont-Nivet, G., 2012. On the influence of diagenesis on the original petrographic composition of Miocene–Pliocene fluvial sandstone in the Himalayan foreland basin of western-central Nepal. J. Asian Earth Sci. 44, 107–116.

Hakimi, M.H., Shalaby, M.R., Abdullah, W.H., 2012. Diagenetic characteristics and reservoir quality of the Lower Cretaceous Biyadh sandstones at Kharir oilfield in the western central Masila Basin, Yemen. J. Asian Earth Sci. 51, 109–120.

Hall, J.S., Mozley, P., Davis, J.M., Roy, N.D., 2004. Environments of Formation and Controls on Spatial Distribution of Calcite Cementation in Plio-Pleistocene Fluvial Deposits, New Mexico, U.S.A. J. Sediment. Res. 74, 643–653.

Hirst, J.P.P., Nichols, G.J., 1986. Thrust tectonic controls on Miocene alluvial distribution patterns, southern Pyrenees., in: Allen, P.A., Homewood, P. (Eds.), Foreland Basins. International Association of Sedimentologists Special Publication, pp. 153–164.

Horton, B.K., Decelles, P.G., 2001. Modern and ancient fluvial megafans in the foreland basin system of the Central Andes, Southern Bolivia: Implications for drainage network evolution if foldthrust belts. Basin Res. 13, 43–63.

Houseknecht, D.W., 1987. Assessing the relative importance of compaction processes and cementation to reduction of porosity in sandstones. Am. Assoc. Pet. Geol. Bull. 71, 633–642.

Howell, J.A., Martinius, A.W., Good, T.R., 2014. The application of outcrop analogues in geological modelling: a review, present status and future outlook. Geol. Soc. London, Spec. Publ. 387, 1–25.

Huang, Q., Angelier, J., 1989. Fracture spacing and its relation to bed thickness. Geol. Mag. 126, 355–362.

Hudleston, P.J., Treagus, S.H., 2010. Information from folds: A review. J. Struct. Geol. 32, 2042–2071.

Iñigo, J.F., Laubach, S.E., Hooker, J.N., 2012. Fracture abundance and patterns in the Subandean fold and thrust belt, Devonian Huamampampa Formation petroleum reservoirs and outcrops, Argentina and Bolivia. Mar. Pet. Geol. 35, 201–218.

Institut Cartogràfic i Geològic de Catalunya, 2006. Regional geological map of Catalonia. https://www.icgc.cat/en/Public-Administration-and-Enterprises/Downloads/Geological-and-geothematic-cartography/Geological-cartography/Geological-map-1-50-000/Regional-geological-map-of-Catalonia-1-50-000 (accessed 2.1.21).

Instituto Geológico y Minero de España, 1995. Almacenamiento subterraneo de gas: previabilidad en formaciones detriticas y salinas. http://info.igme.es/ConsultaSID/r.asp?IdDESCRIPTOR=2681 (accessed 3.20.21).

Lai, J., Wang, G., Wang, S., Cao, J., Li, M., Pang, X., Zhou, Z., Fan, X., Dai, Q., Yang, L., He, Z., Qin, Z., 2018. Review of diagenetic facies in tight sandstones: Diagenesis, diagenetic minerals, and prediction via well logs. Earth-Science Rev. 185, 234–258.

Liu, C., Zhang, R., Zhang, H., Wang, J., Mo, T., Wang, K., Zhou, L., 2017. Genesis and reservoir significance of multi-scale natural fractures in Kuqa foreland thrust belt, Tarim Basin, NW China. Pet. Explor. Dev. 44, 495–504.

Luzón, A., 2001. Análisis tectosedimentario de los materiales terciarios continentales del sector central de la cuenca del Ebro (provincias de Huesca y Zaragoza) (Ph.D. thesis). Zaragoza University, Zaragoza.(in Spanish).

Luzón, A., 2005. Oligocene–Miocene alluvial sedimentation in the northern Ebro Basin, NE Spain: Tectonic control and palaeogeographical evolution. Sediment. Geol. 177, 19–39.

Mann, P., Gahagan, L., Gordon, M.B., 2003. Tectonic setting of the world's giant oil fields, in: Halbouty, M..

(Ed.), Giant Oil and Gas Fields of the Decade 1990–1999. AAPG Memoir, 78, pp. 15–105.

Martin, B., Owen, A., Nichols, G.J., Hartley, A.J., Williams, R.D., 2021. Quantifying downstream, vertical and lateral variation in fluvial deposits: Implications from the Huesca distributive fluvial system. Front. Earth Sci. 8, 564017. https://doi.org/10.3389/feart.2020.564017

Martínez-Martínez, J.M., Soto, J.I., Balanyá, J.C., 2002. Orthogonal folding of extensional detachments: Structure and origin of the Sierra Nevada elongated dome (Betics, SE Spain). Tectonics 21, 1–22.

Morad, S., Al-Ramadan, K., Ketzer, J.M., De Ros, L.F., 2010. The impact of diagenesis on the heterogeneity of sandstone reservoirs: A review of the role of depositional fades and sequence stratigraphy. Am. Assoc. Pet. Geol. Bull. 94, 1267–1309.

Moscariello, A., 2005. Exploration potential of the mature Southern North Sea basin margins: some unconventional plays based on alluvial and fluvial fan sedimentation models. Geol. Soc. London, Pet. Geol. Conf. Ser. 6, 595–605.

Moscariello, A., 2018. Alluvial fans and fluvial fans at the margins of continental sedimentary basins: geomorphic and sedimentological distinction for geo-energy exploration and development. Geol. Soc. London, Spec. Publ. 440, 215–243.

Muñoz, J.A., 1992. Evolution of a continental collision belt: ECORS-Pyrenees crustal balanced cross-section, in: McClay, K.R. (Ed.), Thrust Tectonics. Springer, Dordrecht, pp. 235–246.

Nichols, G., 2005. Tertiary alluvial fans at the northern margin of the Ebro Basin: a review. Geol. Soc. London, Spec. Publ. 251, 187–206.

Nichols, G.J., Hirst, J.P., 1998. Alluvial fans and fluvial distributary systems, Oligo-Miocene, northern Spain; contrasting processes and products. J. Sediment. Res. 68, 879–889.

Puigdefàbregas, C., Munñz, J.A., Marzo, M., 1986. Thrust belt development in the eastern Pyrenees and related depositional sequences in the southern foreland basin., in: Allen, P.A., Homewood, P. (Eds.), Foreland Basins. International Association of Sedimentologists Special Publication, pp. 229–246.

Puigdefàbregas, C., Muñoz, J.A., Vergés, J., 1992. Thrusting and foreland basin evolution in the Southern Pyrenees, in: McClay, K.R. (Ed.), Thrust Tectonics. Springer, Dordrecht, pp. 247–254.

Riba, O., 1976. Syntectonic unconformities of the Alto Cardener, Spanish Pyrenees: a genetic interpretation. Sediment. Geol. 15, 213–233.

Roure, F., Choukroune, P., Berastegui, X., Munoz, J.A., Villien, A., Matheron, P., Bareyt, M., Seguret, M., Camara, P., Deramond, J., 1989. Ecors deep seismic data and balanced cross sections: Geometric constraints on the evolution of the Pyrenees. Tectonics 8, 41–50.

Sáez, A., 1987. Estratigrafía y sedimentología de las formaciones lacustres del tránsito Eoceno-Oligoceno del NE de la Cuenca del Ebro (Ph.D. thesis). University of Barcelona, Barcelona.(in Spanish).

Sáez, A., Anadón, P., Herrero, M.J., Moscariello, A., 2007. Variable style of transition between Palaeogene fluvial fan and lacustrine systems, southern Pyrenean foreland, NE Spain. Sedimentology 54, 367–390.

Scherer, M., 1987. Parameters influencing porosity in sandstones: A model for sandstone porosity prediction. Am. Assoc. Pet. Geol. Bull. 71, 485–491.

Schneider, C.A., Rasband, W.S., Eliceiri, K.W., 2012. NIH Image to ImageJ: 25 years of image analysis. Nat. Methods 9, 671–675.

Serra-Kiel, J., Mató, E., Saula, E., Travé, A., Ferràndez-Canadell, C., Busquets, P., Samsó, J.M., Tosquella, J., Barnolas, A., Àlvarez-Pérez, G., Franquès, J., Romero, J., 2003a. An inventory of the marine and transitional Middle/Upper Eocene deposits of the Southeastern Pyrenean Foreland Basin (NE Spain). Geol. Acta 1, 201–229.

Serra-Kiel, J., Travé, A., Mató, E., Saula, E., Ferràndez-Canadell, C., Busquets, P., Tosquella, J., Vergés, J., 2003b. Marine and transitional Middle/Upper Eocene units of the southeastern pyrenean foreland basin (NE Spain). Geol. Acta 1, 177–200.

Sun, X., 2018. Pore structure characterization of low permeability and tight sandstone reservoirs of Huagang Formation in Xihu Depression (Ph.D. thesis). China University of Petroleum (East China), Qingdao.(in Chinese with English abstract).

Sun, X., Alcalde, J., Gomez-Rivas, E., Struth, L., Johnson, G., Travé, A., 2020. Appraisal of CO2 storage potential in compressional hydrocarbon-bearing basins: Global assessment and case study in the Sichuan Basin (China). Geosci. Front. 11, 2309–2321.

Sun, X., Gomez-Rivas, E., Alcalde, J., Martín-Martín, J.D., Ma, C., Muñoz-López, D., Cruset, D., Cantarero, I., Griera, A., Travé, A., 2021. Fracture distribution in a folded fluvial succession: the Puig-reig anticline (South-eastern Pyrenees). EarthArXiv. doi.org/10.31223/X5J31S

Suppe, J., Sàbat, F., Anton Muñoz, J., Poblet, J., Roca, E., Vergés, J., 1997. Bed-by-bed fold growth by kink-band migration: Sant llorenç de Morunys, eastern Pyrenees. J. Struct. Geol. 19, 443–461.

Taylor, K.G., Machent, P.G., 2011. Extensive carbonate cementation of fluvial sandstones: An integrated outcrop and petrographic analysis from the Upper Cretaceous, Book Cliffs, Utah. Mar. Pet. Geol. 28, 1461–1474.

Taylor, T.R., Giles, M.R., Hathon, L.A., Diggs, T.N., Braunsdorf, N.R., Birbiglia, G. V., Kittridge, M.G., MacAulay, C.I., Espejo, I.S., 2010. Sandstone diagenesis and reservoir quality prediction: Models,

myths, and reality. Am. Assoc. Pet. Geol. Bull. 94, 1093–1132.

Travé, A., Calvet, F., Sans, M., Vergés, J., Thirlwall, M., 2000. Fluid history related to the Alpine compression at the margin of the south-Pyrenean Foreland basin: The El Guix anticline. Tectonophysics 321, 73–102.

Travé, A., Labaume, P., Calvet, F., Soler, A., 1997. Sediment dewatering and pore fluid migration along thrust faults in a foreland basin inferred from isotopic and elemental geochemical analyses (Eocene southern Pyrenees, Spain). Tectonophysics 282, 375–398.

Travé, A., Labaume, P., Vergés, J., 2007. Fluid systems in foreland fold-and-thrust belts: An overview from the southern Pyrenees, in: Lacombe, O., Lavé, J., Roure, F., Vergés, J. (Eds.), Thrust Belts and Foreland Basins. Springer, Berlin, Heidelberg, pp. 93–115.

Valloni, R., Zuffa, G.G., 1984. Provenance changes for arenaceous formations of the northern Apennines, Italy. Geol. Soc. Am. Bull. 95, 1035–1039.

Ventra, D., Clarke, L.E., 2018. Geology and geomorphology of alluvial and fluvial fans: current progress and research perspectives. Geol. Soc. London, Spec. Publ. 440, 1–21.

Vergés, J., 1993. Estudi geològic del vessant sud del Pirineu oriental i central. Evolució cinemàtica en 3D (Ph.D. thesis). University of Barcelona, Barcelona.(in Spanish).

Vergés, J., 2007. Drainage Responses to Oblique and Lateral Thrust Ramps: A Review, in: Nichols, G., Paola, C., Williams, E.A. (Eds.), Sedimentary Processes, Environments and Basins: A Tribute to Peter Friend. International Association of Sedimentologists Special Publication, pp. 29–47.

Vergés, J., Marzo, M., Muñoz, J.A., 2002. Growth strata in foreland settings. Sediment. Geol. 146, 1–9.

Vergés, J., Marzo, M., Santaeulària, T., Serra-Kiel, J., Burbank, D.W., Muñoz, J.A., Giménez-Montsant, J., 1998. Quantified vertical motions and tectonic evolution of the SE Pyrenean foreland basin. Geol. Soc. London, Spec. Publ. 134, 107–134.

Vergés, J., Muñoz, J.A., Martínez, A., 1992. South Pyrenean fold and thrust belt: The role of foreland evaporitic levels in thrust geometry, in: K.R., M. (Ed.), Thrust Tectonics. Springer, Dordrecht, pp. 255–264.

Vincent, S.J., 2002. The Sis palaeovalley: a record of proximal fluvial sedimentation and drainage basin development in response to Pyrenean mountain building. Sedimentology 48, 1235–1276.

Wang, H., Ma, F., Tong, X., Liu, Z., Zhang, X., Wu, Z., Li, D., Wang, B., Xie, Y., Yang, L., 2016. Assessment of global unconventional oil and gas resources. Pet. Explor. Dev. 43, 925–940.

Wang, Z., Lü, X., Wang, S., Li, Y., Zhou, X., Quan, H., Li, R., 2020. Fracture systems and petrophysical

properties of tight sandstone undergoing regional folding: A case study of the Cretaceous reservoirs in the Kuqa foreland thrust belt, Tarim Basin. Mar. Pet. Geol. 111, 104055. https://doi.org/10.1016/j.marpetgeo.2019.104055

Watkins, H., Butler, R.W.H., Bond, C.E., Healy, D., 2015. Influence of structural position on fracture networks in the Torridon Group, Achnashellach fold and thrust belt, NW Scotland. J. Struct. Geol. 74, 64–80.

Watkins, H., Healy, D., Bond, C.E., Butler, R.W.H., 2018. Implications of heterogeneous fracture distribution on reservoir quality; an analogue from the Torridon Group sandstone, Moine Thrust Belt, NW Scotland. J. Struct. Geol. 108, 180–197.

Weissmann, G.S., Hartley, A.J., Scuderi, L.A., Nichols, G.J., Davidson, S.K., Owen, A., Atchley, S.C., Bhattacharyya, P., Chakraborty, T., Ghosh, P., Nordt, L.C., Michel, L., Tabor, N.J., 2013. Prograding distributive fluvial systems—geomorphic models and ancient examples, in: Driese, S.G., Nordt, Lee C. (Eds.), New Frontiers in Paleopedology and Terrestrial Paleoclimatology: Paleosols and Soil Surface Analog Systems. SEPM Special Publication, pp. 131–147.

Weissmann, G.S., Hartley, A.J., Scuderi, L.A., Nichols, G.J., Owen, A., Wright, S., Felicia, A.L., Holland, F., Anaya, F.M.L., 2015. Fluvial geomorphic elements in modern sedimentary basins and their potential preservation in the rock record: A review. Geomorphology 250, 187–219.

Wennberg, O.P., Azizzadeh, M., Aqrawi, A.A.M., Blanc, E., Brockbank, P., Lyslo, K.B., Pickard, N., Salem, L.D., Svånå, T., 2007. The Khaviz Anticline: an outcrop analogue to giant fractured Asmari Formation reservoirs in SW Iran. Geol. Soc. London, Spec. Publ. 270, 23–42.

Williams, E.A., Ford, M., Vergés, J., Artoni, A., 1998. Alluvial gravel sedimentation in a contractional growth fold setting, Sant Llorenç de Morunys, southeastern Pyrenees. Geol. Soc. London, Spec. Publ. 134, 69–106.

Yuste, A., Luzón, A., Bauluz, B., 2004. Provenance of Oligocene-Miocene alluvial and fluvial fans of the northern Ebro Basin (NE Spain): An XRD, petrographic and SEM study. Sediment. Geol. 172, 251–268.

Zhang, R., Yao, G., Shou, J., Zhang, H., Tian, J., 2011. An integration porosity forecast model of deposition, diagenesis and structure. Pet. Explor. Dev. 38, 145–151.

Zheng, H., Huang, X., Butcher, K., 2006. Lithostratigraphy, petrography and facies analysis of the Late Cenozoic sediments in the foreland basin of the West Kunlun. Palaeogeogr. Palaeoclimatol. Palaeoecol. 241, 61–78.

Zuffa, G.G., 1980. Hybrid arenites: their composition and classification. J. Sediment. Petrol. 50, 21–29.

Zuffa, G.G., 1985. Optical analyses of arenites: Influence of methodology on compositional results, in: Zuffa, G.G. (Ed.), Provenance of Arenites: NATO-Advanced Study Institute Series C. Reidel Publishing Company, Dordrecht, pp. 165–189.